RADC-TDR-64-398
Final Report

A STUDY OF SEVERAL MICROWAVE COMPRESSION FILTER TECHNIQUES

TECHNICAL DOCUMENTARY REPORT NO. RADC-TDR-64-398

November 1964

Intelligence Application Branch
Rome Air Development Center
Research and Technology Division
Air Force Systems Command
Griffiss Air Force Base, New York

Project No. 4505 , Task No. 450501

(Prepared under Contract AF 30(602)-2985 by Systems Techniques Laboratory, Stanford Electronics Laboratories, Stanford University, Stanford, California. Authors: H.S. Hewitt, W.R. Kincheloe, Jr. and M.H. Musser.)

ABSTRACT

Linear passive filters which decrease the duration of a frequency modulated pulse (''pulse compression'' filters) are finding increasing application in radar and scanning receiver systems. This report describes the design, construction, and performance of several compression filters intended for use in a particular scanning receiver. These filters were designed to compress pulses in which the frequency varies linearly with time between 1 Gc. and 2 Gc., nominally at a rate of 2×10^{16} cycles/sec.^{2} (20 Megacycles per second per nanosecond).

Included in the discussion are the following filter types:

1. Dispersive Helix
2. Folded Tape Meander Line (FTML)
3. Printed Circuit Meander Line (PCML)
4. Tapped Delay Line (TDL)
5. Radiation-Coupled Tapered Meander Line (TML)

A description of the construction techniques and performance of the FTML, the PCML, and the TML is included in this report, while the Helix and FTML are described in separate reports issued under this contract. The intent of this report is not to exhaustively treat each type of filter, but rather to provide a variety of possible approaches to compression filter realization, to provide design information, and to weigh some of the advantages and disadvantages of each type of filter.

Although the filters described here are designed for a particular scan rate and frequency range, a similar approach could be used over a wide range of system parameters. With this in mind, an effort has been made to present design data in such a way as not to limit its generality or applicability.

AIR FORCE, Cato Show Prtg. Co. 11/13/64 - 141

PUBLICATION REVIEW

This report has been reviewed and is approved. For further technical information on this project, contact Mr. L. B. Sues, RADC (EMIAD), Ext. 75276.

Approved: Lawrence B. Sues
LAWRENCE B. SUES
Task Engineer

Approved:
ROBERT J. QUINN, JR.
Colonel, USAF
Chief, Intelligence & Information Processing Div

FOR THE COMMANDER: Irving J. Gabelman
IRVING J. GABELMAN
Chief, Advanced Studies Group

TABLE OF CONTENTS

TABLE OF CONTENTS (Cont.)

LIST OF ILLUSTRATIONS

LIST OF ILLUSTRATIONS (Cont.)

LIST OF ILLUSTRATIONS (Cont.)

List of Frequently Used Symbols & Abbreviations

A	Dimensional parameter
b	Bandwidth in cps (or Gc where specified) also dimensional parameter in Chap. 4.
B	Percentage bandwidth (Bandwidth/center frequency)
c	Velocity of light in vacuum
c_d	Velocity of light in dielectric
d	duration of time function in seconds
D	Dimensional parameter
e(t)	Filter excitation Function
E(t)	Envelope of e(t)
E(f)	Filter excitation spectrum function
f	Frequency in cps
H(f)	Filter spectrum function
j	$\sqrt{-1}$
k	Boltzmann's constant or phase change coefficient (ω/c)
k^1	Voltage coupling coefficient
K	Time bandwidth product (bd)
L	Dimensional parameter
PCML	Printed circuit meander line
r(t)	Filter output function
s	Width of gap between two coupled strips
S	Scan rate in cycles per sec^2.

List of Frequently Used Symbols & Abbreviations

t	Time in seconds
Δt	Time required to scan filter bandwidth in seconds
TDL	Tapped delay line
TML	Tapered meander line
v_g	Group velocity of signal
w	Dimensional parameter
W	Dimensional parameter
Z_o	Characteristic impedance
Z_{oe}	Even-mode coupled-line impedance
Z_{oo}	Odd-mode coupled-line impedance
α	Phase constant in cycles
β	Phase change per unit length
ϵ_r	Dielectric constant relative to that of vacuum
θ	Phase change per half-period of slow-wave structure
λ	Wavelength
τ	Group time delay in seconds
ϕ	Phase constant in cycles
Φ	Phase function in cycles
ω	Radian frequency

I. INTRODUCTION

A. OBJECTIVE

The basic component in a pulse compression system is the filter which actually does the compressing. System performance is usually dependent upon the accuracy with which the desired filter characteristics can be achieved. It was the objective of this project to investigate several approaches to compression filter design to determine their relative suitability for use in a pulse compression system. This should increase the number of filter types available to choose from when designing such a system.

Of the five filter types studied in this project, three are discussed in this report and two are analyzed in individual reports*. All five of these filter types were developed to compress a pulse scanning between 1 Gc. and 2 Gc. at a constant scan rate of 2×10^{16} cycles/sec^2, this choice of parameters being dictated by test equipment available.

B. PERFORMANCE CRITERIA

The theory of pulse compression has been developed extensively in the literature** and will not be covered in detail here. Only those equations useful in describing compression filter performance will be presented and the sources of the development will be indicated as references.

---

* Ref. 1 and 2

** Examples of literature on the subject of pulse compression theory and techniques can be found in Refs. 3 through 6. A useful bibliography is included in Ref. 3.

Considering only the case for constant scan rate, the frequency of the input pulse is

$$f_S = f_O + St \tag{1.1}$$

where

f_s = frequency of input pulse, cps

f_O = frequency at t = O in cps

$S = \frac{df}{dt}$ = scan rate in cycles/sec.^{2}

The phase is the time integral of f:

$$\Phi_s = \int f_s dt = f_0 t + \frac{1}{2} S t^2 + \phi_0 \tag{1.2}$$

where

Φ_s = phase of input pulse in cycles

ϕ_0 = phase at t = O in cycles

The input pulse is given by

$$e(t) = E(t) e^{j2\pi\Phi_s} \tag{1.3}$$

where

E(t) = envelope of e(t)

A filter to compress e(t) should have the delay characteristic (Ref. 3)

$$\tau_f = \tau_0 - \frac{f}{S} \tag{1.4}$$

where

τ_f is the group delay of the compression filter

τ_0 is a constant delay, sec.

S is scan rate, cycles/sec.^{2}

Taking the frequency integral to obtain filter phase in cycles,

$$\Phi_f = \int \tau_f df = \tau_0 f - \frac{f^2}{2S} + \alpha \tag{1.5}$$

where α is a phase constant. The compression filter for a quadratic phase excitation is seen to possess a quadratic phase term. The filter is

said to be phase matched when the coefficient of the quadratic phase term in the input signal is equal to one fourth the negative reciprocal of the quadratic filter phase term* (phase in cycles for both terms).

The output of the compression filter is the inverse Fourier transform of the product of the filter impulse response and the spectrum function of the input signal:

$$r(t) = \int_{-\infty}^{\infty} H(f)E(f)e^{j2\pi ft}dt \qquad (1.6)$$

where

r(t) is the filter output time function

H(f) is the filter spectrum function

E(f) is the spectrum function of the filter excitation

The expression representing the desired filter response when the filter is phase-matched can be determined with Eq. (1.6):**

$$\left|r(t-\tau)\right| \cong \sqrt{\frac{1}{8S}}\ a_1\ \left|a_2(t)\right| \qquad (1.7)$$

where

$\left|r(t-\tau)\right|$ is the response envelope displaced in time by amount τ

a_1 is the amplitude of the excitation (a_1 = constant)

$a_2(t)$ is the magnitude function of the filter impulse response

Equation (1.7) illustrates the fact that the compressed output pulse has the form of the impulse response of the filter when the phase-matched condition exists over the entire filter bandwidth. The amplitude of the response is proportional to the excitation amplitude and inversely proportional to $\sqrt{S}$.

---

* A phase matching parameter η has been defined in Ref. 3 where filter performance is related to various values of η corresponding to excitation scan rates which differ from that for which the filter is designed to match.

** Ref. 3, Eq. (3.30)

The filters discussed in this report were all designed for use in a frequency-translation receiver system in which the signal to be analyzed is combined in a mixer with the output of a scanning local oscillator. The translated (in frequency) signal is compressed by the compression filter, the compressed output pulse defining the signal spectrum on a frequency-calibrated time scale. As seen from Eq. (1.7), it is possible to exercise some control over the shape and width (in time) of the compressed pulse in order to provide better analysis of the signal spectrum. For example, improved resolution of adjacent signals of different amplitudes might be obtained with rectangular compressed pulses, and these represent the impulse response of a sin x/x bandpass shape.

In the case of the scanning spectrum analyzer, it is usually desirable to make the compression filter bandwidth as large as possible while maintaining the phase matched condition over the entire filter bandwidth. This will result in a shorter compressed pulse (smaller d, where d is the duration of the compressed pulse) due to the Fourier transform relationship between filter bandwidth and d. The resolution in cps is

$$Sd = K_2\left(\frac{S}{b\Delta t}\right)^{1/2} \tag{1.8}$$

where b is the compression filter bandwidth, $K_2 = bd$ and is a function of the shape of the filter spectrum envelope shape and Δt is the time required to scan the filter bandwidth.

It is seen that for a given scan rate and envelope shape (K_2 = constant), the resolution of the compression filter is proportional to $(b\Delta t)^{-1/2}$. The factor $b\Delta t$ is a useful quantity in evaluating the relative merits of compression filters and will be referred to as the time-bandwidth product of the filter.

The time-bandwidth product also appears in the expression for the signal-to-noise ratio of a scanning spectrum analyzer*:

* This is a restatement of Eq. (3.29), Reference 3

$$\left(\frac{r_1}{e_n}\right)^2 = \frac{1}{8FkT} \cdot \frac{a_1^2}{K_2 R} \cdot \left| \frac{b\Delta t D}{b+B} \right|^{1/2} \tag{1.9}$$

where

$$e_n = A_{2m}(FkTRb_n)^{1/2} \tag{1.10}$$

$A_{2m} = \left|H(w)\right|_{max}$ = max. value of filter spectrum envelope

F is the analyzer noise figure

k is Boltzmann's constant

R is the equivalent source resistance

$b_n = b$ = noise bandwidth

B is the total signal spectrum scanned

D is the time taken to scan the signal spectrum plus the filter bandwidth ($D = \frac{b+B}{S}$)

For the case where the analyzer is scanning a much larger total bandwidth than that of the filter $(B >> b)$, the signal to noise ratio is proportional to $(b\Delta t)^{1/2}$.

These equations provide the performance factors by which the compression filters are compared. The time-bandwidth product is a measure of the potential noise performance as well as frequency resolution capabilities in a scanning analyzer system. The degree to which the filter phase characteristic matches that of the scanning excitation (the "phase-matching" parameter) is a useful performance factor. A mismatch in the phase characteristic will generally cause a "spreading" of the compressed pulse since the Fourier transform relationship between the envelope of the filter spectrum function and the compressed pulse no longer exists.

Another performance factor of interest is the peak-to-sidelobe ratio. This can be defined as the ratio of the amplitude of the compressed pulse to the amplitude of the next largest peak. In a scanning spectrum analyzer system, this is a measure of the ability of the system to resolve adjacent signals of different amplitudes. Anything which affects

the phase-matching of the filter can have an adverse effect on the peak-to-sidelobe ratio.

A means of predicting the spurious sidelobes induced in the filter output by errors in the phase-matching is given in References 6 and 7 and is known as the paired-echo concept. An additional spurious response due to errors in the filter envelope shape can be predicted using this concept. For the purposes of this brief treatment of paired-echo theory, a spurious response will be defined as the departure of the compression filter output from the output that would be obtained from an ideal (phase-matched with desired spectrum envelope shape) system.

If the pulse representing the response of an ideal compression system is passed through a network which has a transfer characteristic containing all the phase and amplitude errors present in an actual system, the total response should be the same as it would be from a compression system containing phase and amplitude errors. Thus for a system containing no errors, the amplitude characteristic would be unity and the phase would be a linear function of frequency (ideal transmission line).

Considering first the case in which only phase distortion is present, an expression containing a sinusoidal phase error term is written:

$$e_m(t) = e(t) \exp\left[j b_1 \sin(\omega_m t + \phi) \right] \tag{1.11}$$

where

$e(t)$ = undistorted excitation function

b_1 = peak phase error in radians

$\omega_m = 2\pi f_m$ = frequency of phase error

ϕ = arbitrary phase positioning factor

The composite compression filter output is:

$$\begin{aligned} r(t) = {} & J_0(b_1)\, r(t) \cos \omega_0 t \\ & + \sum k_n J_n(b_1) \left\{ r\left(t + \frac{n\omega_m}{\Delta\omega} T\right) \cos\left[\left(\omega_0 + \frac{n\omega_m}{2}\right) t + n\phi \right] \right. \\ & \left. + (-1)^n r\left(t - \frac{n\omega_m}{\Delta\omega} T\right) \cos\left[\left(\omega_0 - \frac{n\omega_m}{2}\right) t - n\phi \right] \right\} \end{aligned} \tag{1.12}$$

where

$\Delta\omega = 2\pi\Delta f$, linear swept bandwidth

T = uncompressed pulse duration

$r(t)$ = compressed pulse envelope function

k_n = weighting factor of passband frequency response

$J_n(b_1)$ = the n^{th} order Bessel function of argument b_1

ω_0 = excitation frequency when $t = 0$

Equation (1.12) indicates that the compressed pulse is flanked by symmetrically spaced pairs of signals of peak amplitude $J_n(b_1)$. The time interval separating the n^{th} set of paired signals is

$$\frac{\Delta t}{n} = \frac{\omega_m}{\Delta\omega} T = \frac{f_m}{\Delta f} T \qquad (1.13)$$

Since $\left(\frac{1}{\Delta f}\right) \cong d$, the compressed pulse width, Eq. (1.13) can be restated:

$$\Delta t = n(f_m T) \cdot d \qquad (1.14)$$

This indicates that an error term with $f_m T$ cycles of error modulation during time T will cause echoes of amplitude $J_n(b_1)$ to appear at the filter output separated from the compressed pulse by $\pm \frac{\Delta t}{2}$. By the use of several different error frequencies with arbitrary phase ϕ, the effect of a wide variety of phase errors in a pulse compression system can be studied.* The paired echoes resulting from errors in the filter magnitude function are similar to those caused by phase errors and are described in Reference 6 in the discussion of paired echo theory.

In the case of the scanning spectrum analyzer, the ability to resolve adjacent signals of different amplitudes is limited by the presence of errors in the system. These errors create echo responses which are identical in shape to the response to an actual signal of smaller amplitude

---

* This is described in detail in Reference 7

and different frequency than the original.

In practice, the problem of constructing a compression filter with the desired amplitude and phase characteristics is a difficult one. All of the filters constructed under this project have exhibited errors in these characteristics and as a result, the maximum peak-to-sidelobe ratio attained is 15 db.

C. FILTER TYPES

A filter capable of compressing a linearly frequency modulated signal can generally be classified into one of four main groups. These are:

1. The continuously dispersive transmission line (helix, meander line, etc).
2. The tapped delay line with dispersive taps (each tap has compression filter of small time-bandwidth product).
3. The tapped delay line with non-dispersive bandpass filters at each tap.
4. The tapped delay line with no filters on the taps.

The only filter constructed under this project which is not included in type one was the tapped delay line with resonant-loop couplers (Section III).

D. MEASUREMENTS

A straightforward method of measuring the performance of a compression filter is to insert it into a compression system matched to its parameters and observe the compression characteristics. Unfortunately, an exactly linear sweep cannot be generated with presently available techniques at the high scan rates for which the compression filters studied here are designed. The filter output represents a resultant of sweep and filter errors which make the determination of the error source difficult.

If a filter performs well in a compression system in which sweep errors exist, it indicates that the filter is both insensitive to these errors and accurately matched in phase to the average excitation phase. If, however, the filter fails to perform well, this could be due to either poor phase matching or great sensitivity to scan rate errors. It is necessary to measure the phase characteristics of the filter to discover whether poor performance is due to incorrect filter design or to a filter which is highly sensitive to error.

The filters studied here are designed for fifty nanoseconds differential delay from one to two Gc. This results in a relative phase shift of seventy-five cycles over the one Gc. range. A satisfactory way to measure this large phase shift is at the "Phase Bridge,"* Figure 1.

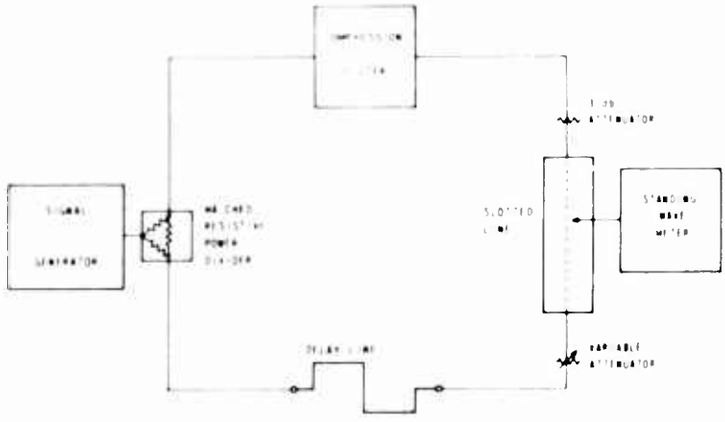

Figure 1 Phase Bridge for Measuring Many Cycles of Phase Shift Over a Large Frequency Range.

If the line lengths from the generator to the slotted line are equal, standing wave maximum will appear at the center of the slotted line and will remain stationary as the signal generator frequency is changed. If one of the lines is dispersive, the position of the electrical center of the system will

---

* Described in detail on page 69, Reference 2

change with frequency and the amount of movement will be function of the change of delay through the dispersive line. Due to the square-law characteristic of the slotted-line detector, it is easier to track a null than a voltage maximum, so an attempt is made to track the null nearest the central maximum since this is the one which moves least rapidly with frequency. By carefully following a null as frequency is changed, a plot of phase vs. frequency may be obtained. Nulls which have traveled beyond the range of the slotted line may be tracked by moving the probe to a new null N wavelengths away and tracking the new null while remembering that the desired one is N wavelengths further down the line. The envelope delay, $\frac{d\phi}{d\omega}$, may be obtained with the phase bridge although the measurement becomes tedious if points are to be taken over small frequency increments.

Another technique which gives the phase characteristic to an accuracy of about one-quarter cycle is to measure the impulse response directly. The experimental set-up is shown in Figure 2.

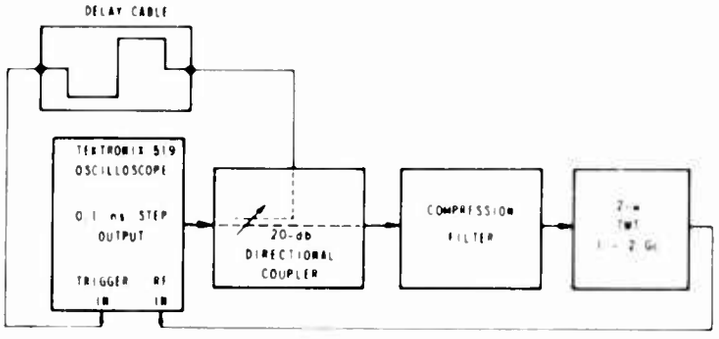

Figure 2. Impulse Method of Measuring Phase Response of Compression Filter

Figure 3. Impulse Response of Typical Compression Filter Measured as Shown in Figure 2.

The observed impulse response as shown in Figure 3 can be expanded by increasing the sweep speed of the oscilloscope and delaying the trigger an amount appropriate to observe the desired portion of the waveform. This method of measurement could conceivably be used to measure dispersion in any frequency range by using heterodyne techniques.

In this report, filter characteristics are evaluated primarily by observing performance in a compression system. The compressed pulse is detected with a detector of sufficient video bandwidth to pass the short-duration pulses. The response is observed and photographed on a sampling oscilloscope and the resulting photographs are used as examples of system performance. Knowing the detector transfer characteristic, the peak-to-sidelobe ratio and the pulse shape may be accurately determined from the photographs.

II. THE PRINTED-CIRCUIT MEANDER LINE

A. DESCRIPTION

The printed-circuit meander line (PCML) is a transmission line which repeatedly folds back upon itself in such a way that coupling takes place between adjacent sections of the line. Figure 4 illustrates a short section of such a line and defines dimensions which will be used in the theoretical development of the line characteristics.

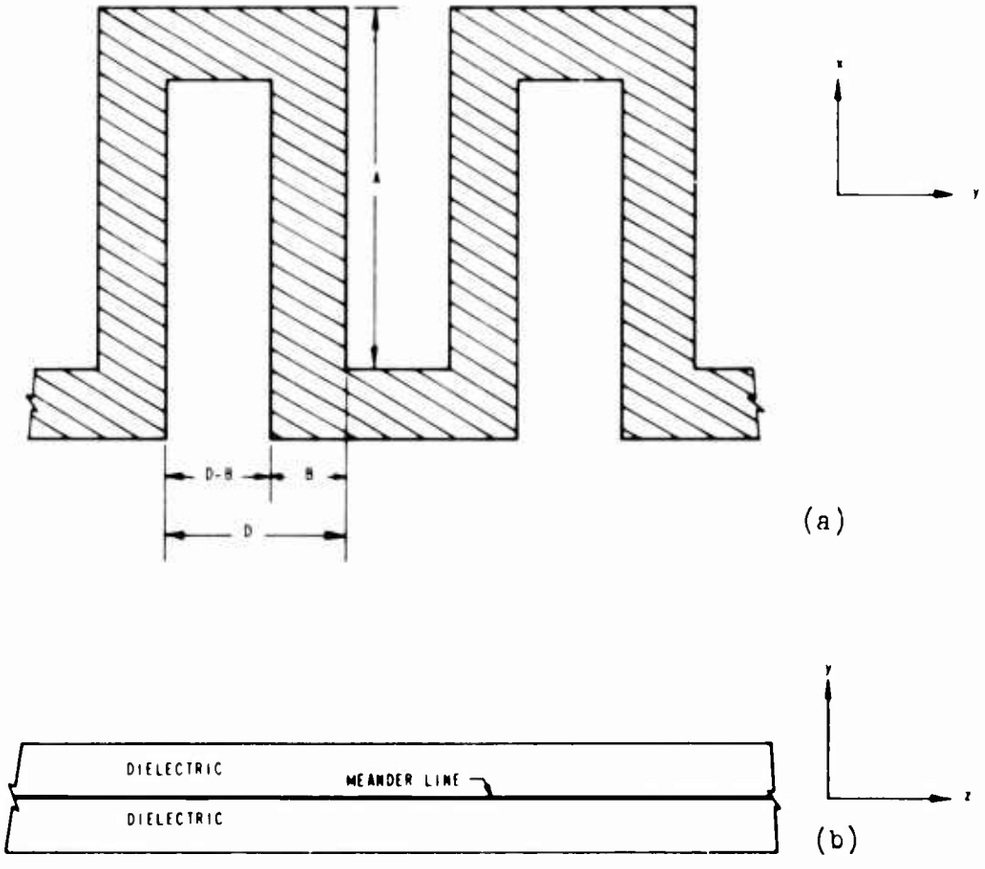

Figure 4. Printed-Circuit Meander Line

(a) Section of Meander Line as Seen with One Dielectric Sheet Removed.
(b) Edge View of Line

Figure 5 is a photograph of one of the three PCML's constructed and illustrates the tapered impedance-matching transformers and the Type N-to-stripline adapters. The ground planes extend only to the end of the transformer sections, leaving the meander line between dielectric sheets with no ground planes. The conductor is 0.0023 in. copper, and the meander line shape is photo-etched from a copper sheet banded to the dielectric.

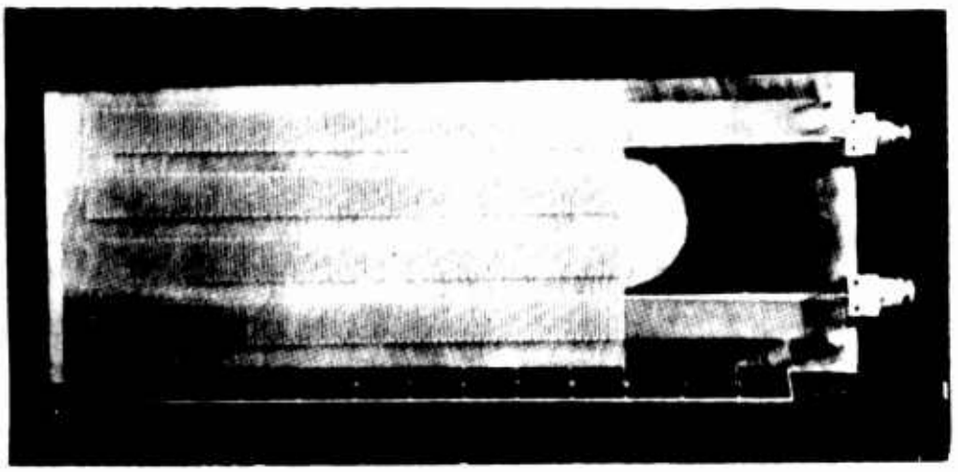

Figure 5. Photograph of PCML, W - 0.040.
The Scale Markings are Inches.

The delay properties of the FTML are a result of coupling between turns of the structure. Figure 6 is a normalized plot of group delay vs frequency for three different values of B/D (Dimensions are shown in Figure 4). Although the over-all delay curve is non-linear, by restricting the frequency range to an octave or less the deviation from linearity can be made small.

B. THEORY

The dispersion relations upon which the PCML design is based are obtained from two papers by P.N. Butcher, References 8 and 9. The basic equation relating phase and frequency is given as Eq. (33a) in Reference 9:

$$\cot^2 \frac{kA}{2} = \tan \frac{\theta}{2} \left[\frac{\Delta U(\frac{B}{D}, \theta)\, \Delta U\left[(1-\frac{B}{D}), \theta+\pi\right]}{\Delta U\left[(1-\frac{B}{D}), \theta\right]\, \Delta U(\frac{B}{D}, \theta+\pi)} \right] \tag{2.1}$$

A, B and D are dimensions defined in Figure 4.

$k = \dfrac{2\pi \times \text{frequency}}{\text{velocity of light in dielectric}}$ = phase change coefficient

θ = phase change per half-period in radians (the period of the structure is 2D).

$$\Delta U\left[(1-\frac{B}{D}), \theta\right] = 2 \int_0^{\alpha} \frac{\cos(1-\frac{\theta}{\pi})t}{\sqrt{\sin^2\alpha - \sin^2 t}}\, dt \tag{2.2}$$

where

$$\alpha = \frac{\pi}{2}(1-\frac{B}{D}) \tag{2.3}$$

Implicit differentiation of Eq. (2.1) combined with certain approximations (Appendix) yields the delay equation from which Figure 6 is plotted.

$$\frac{C_d D}{A v_g} = \frac{\sin^3(\frac{\omega A}{2C_d})}{\cos(\frac{\omega A}{2C_d})} \left[X \sec^3(\frac{\beta D}{2}) + \tan(\frac{\beta D}{2}) \frac{dX}{d\beta} \right] \tag{2.4}$$

c_d is velocity of light in dielectric.

v_g is group velocity on meander line of signal at frequency ω

$\beta = \dfrac{\theta}{D}$ = phase-change per unit length of PCML in z direction (Figure 6).

$$X = \left[\frac{\Delta U(\frac{B}{D}, \theta)\, \Delta U\left[(1-\frac{B}{D}), \theta+\pi\right]}{\Delta U\left[(1-\frac{B}{D}), \theta\right]\, \Delta U(\frac{B}{D}, \theta+\pi)} \right] \tag{2.5}$$

Equation 2.5 and its first derivative have been evaluated at several points for B/D = 0.25 and B/D = 0.75. The case for B/D = 0.5 is of particular interest due to the fact that X becomes equal to unity thus simplifying the evaluation of Eq. (2.4).

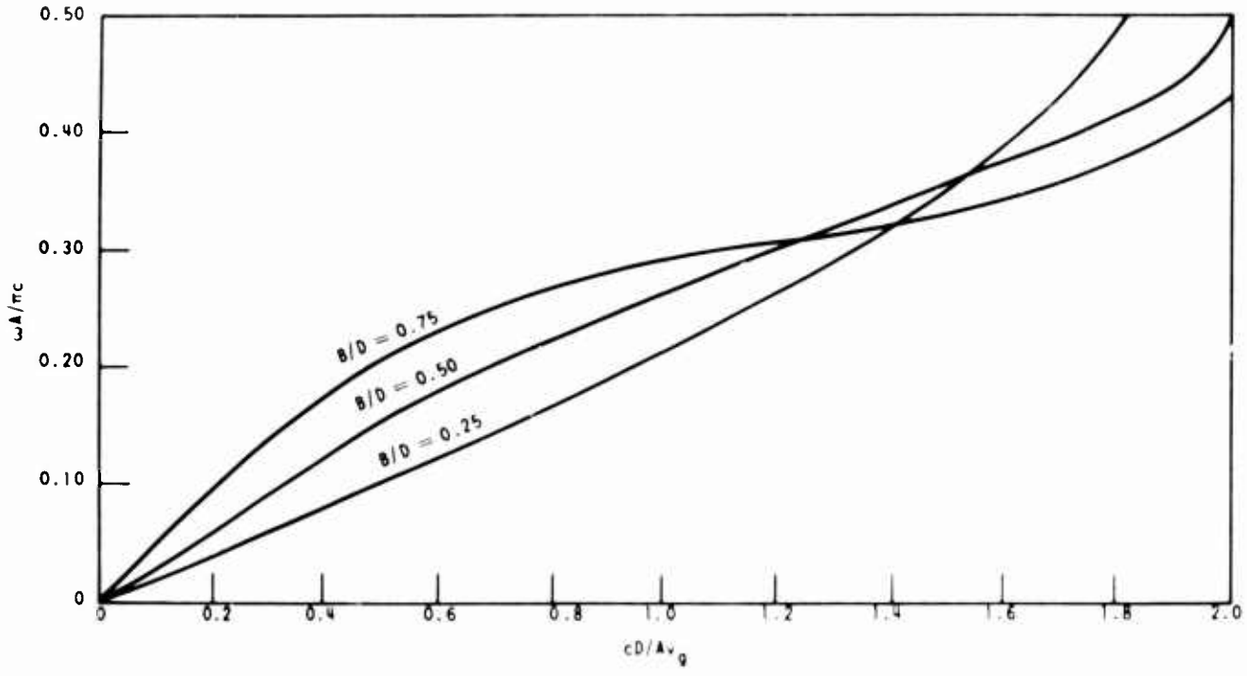

Figure 6. Normalized Group Delay vs Normalized Frequency for Various Values of W/D.

C. DESIGN AND CONSTRUCTION

For a given time-bandwidth product, one of the curves represented by Figure 6 must be matched to a straight line over the desired frequency range. The three filters described here were all matched to the B/D = 0.5 curve between $\frac{A\omega}{\pi C_d} = 0.2$ and $\frac{A\omega}{\pi C_d} = 0.4$. This range of values was picked because, for the three curves drawn, it appeared to be the best compromise between large delays (thus allowing shorter line lengths for a given delay) and linearity of delay vs frequency for the desired octave bandwidth.

For each of the three filters,

$$\frac{A\omega}{\pi C_d} = 0.2 \text{ for } \frac{\omega}{2\pi} = 1 \text{ Gc} \tag{2.6}$$

$$\frac{A\omega}{\pi C_d} = 0.4 \text{ for } \frac{\omega}{2\pi} = 2 \text{ Gc} \tag{2.7}$$

which results in

$$A = \frac{0.2\pi c}{\omega\sqrt{\epsilon_r}} = \frac{3.0}{\sqrt{\epsilon_r}} \text{ cm} \tag{2.8}$$

C is velocity of light in vacuum

ϵ_r is relative dielectric constant

To determine the length of the PCML, the equation relating differential delay to group velocity is used:

$$\Delta T = L\left(\frac{1}{v_{g2}} - \frac{1}{v_{g1}}\right) \tag{2.9}$$

ΔT = (filter group delay at F = 2 Gc.) - (filter group delay at F = 1 Gc.)

v_{g2} = group velocity at F = 2 Gc.

v_{g1} = group velocity at F = 1 Gc.

L = total length of meander line

From Figure 6, $1/v_{g2}$ and $1/v_{g1}$ are obtained:

$$\frac{1}{v_{g2}} = 1.74\left(\frac{A}{CD}\right) \tag{2.10}$$

$$\frac{1}{v_{g1}} = 0.69\left(\frac{A}{CD}\right) \tag{2.11}$$

Combining Eqs. (2.6), (2.10), and (2.11) with Eq. (2.9), we obtain:

$$L = \frac{\Delta T}{1.05\left(\frac{10^{-10}}{D}\right)} = 9.52 \times 10^{9} D\Delta T \tag{2.12}$$

To match the PCML to a scan rate S = 2×10^{16} cycles/second^2 and a bandwidth b = 10^9 cycles/second, the desired differential group delay is:

$$\Delta t = \frac{b}{S} = 50 \times 10^{9}\,\text{sec.} \tag{2.13}$$

The value of B is the primary factor governing loss in the filter. The values of B chosen for the three filters were 0.01 in., 0.02 in., and 0.04 in. As expected, the PCML for which B = 0.01 in. had high insertion loss, the attenuation increasing with frequency and having a value of 80 db at 2 Gc.

B was increased to 0.02 in. for the next filter, the object being to reduce loss while still retaining a small structure. This filter had an insertion loss of 40 db at 2 Gc, but had a useful range over 600 Mc. wide centered at 1050 Mc where the loss vs frequency curve was flat within $\pm$ 3 db. Compression of a scanning signal was observed with this filter indicating that the phase characteristic was at least approximately the

desired quadratic.

In an effort to achieve even greater effective filter bandwidth, the third filter was constructed with B = 0.04 in. This filter did not exhibit satisfactory compression characteristics.

	B Inches	D Inches	L Inches	A Inches	Dielectric Material
Filter No. 1	0.010	0.020	9.52	0.740	Polystyrene $\sqrt{\epsilon_r} = 2.55$
Filter No. 2	0.020	0.040	19.04	0.709	Rexolite 2200 $\sqrt{\epsilon_r} = 2.77$
Filter No. 3	0.040	0.080	38.08	0.709	Rexolite 2200 $\sqrt{\epsilon_r} = 2.77$

Figure 7. Dimensions of The Three Meander Line Filters Described in Text.

The construction of the PCML's employs conventional photo-etching techniques. The meander line is drawn to scale with black ink on white paper and photographed. To improve accuracy, the line may be drawn several times actual size and reduced in the photographic process. The resulting negative is used to expose the sensitized copper and the unexposed copper is dissolved from the underlying dielectric with acid leaving the copper meander line remaining.

The material for the first filter, B - 0.01 in., was 0.25 in. thick polystyrene sheet to which a 0.0022 in. copper foil had been bonded. The bonding agent was a pressure sensitive silicone adhesive supplied as a backing on the copper foil and appeared to be unaffected by the etching process.

The second and third filters, B - 0.02 in. and B - 0.04 in., were constructed using the same techniques as the first except that copper-clad Rexolite 2200 was used as the dielectric material.

D. Performance and Measurements

Insertion loss for the three PCML's is shown in Figure 8. The relatively steep slope of the loss vs frequency curve for B = 0.01 in. reduces the effective bandwidth of this filter to much less than the desired 1 Gc. The other two filters also fall short of this figure but have sufficient band-

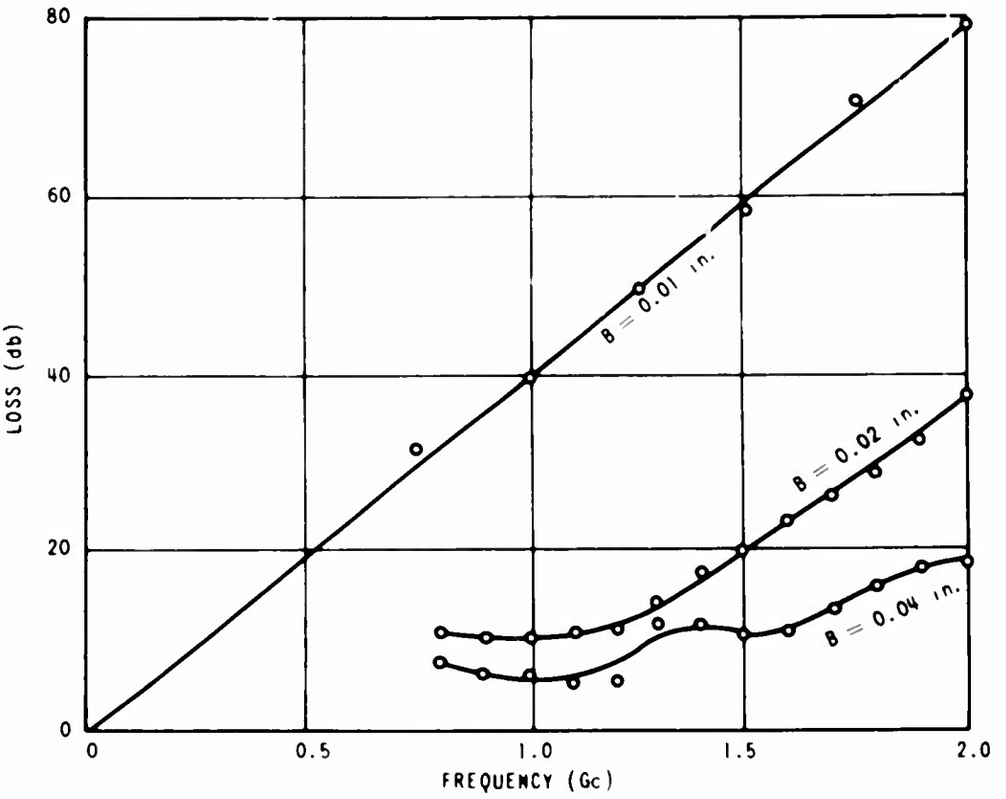

Figure 8. Insertion Loss vs Frequency, PCML

width to be useful.

Due to the high attenuation, the B = 0.01 in. PCML was not tested in a compression system. The third filter, B = 0.04 in., did not exhibit satisfactory compression characteristics and was not pursued further.

The second filter constructed, B = 0.02 inches, provided useful compression as evidenced by Figure 9. The scan rate at which optimum com-

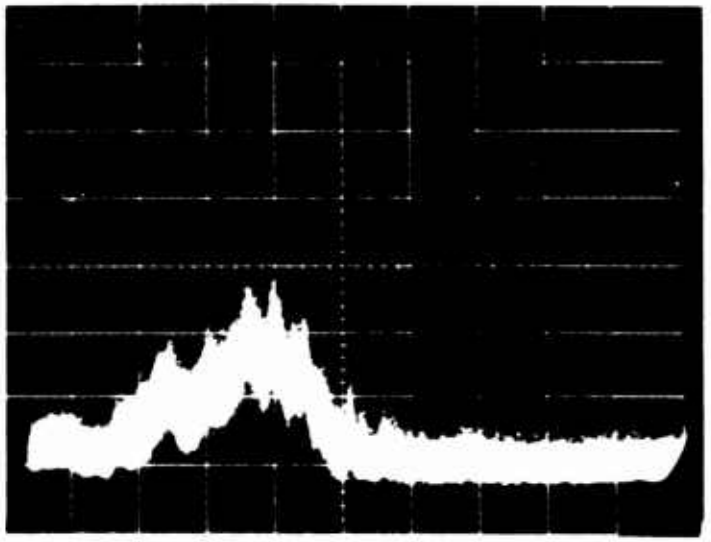

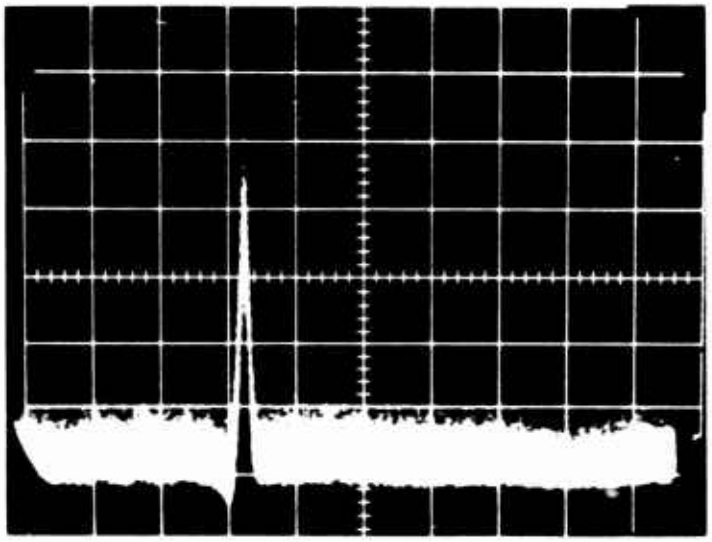

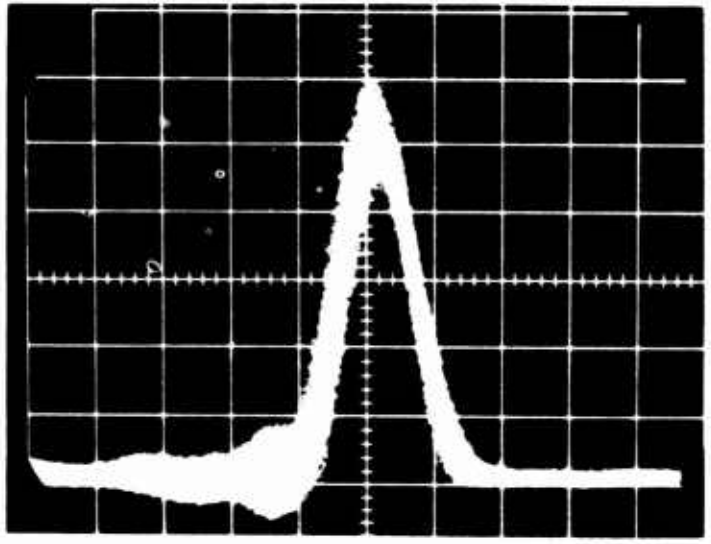

Figure 9. Compression Characteristics of PCML, B - 0.02 in.

(a) Uncompressed pulse envelope at filter imput, S - 3 x 10^{16} cycles/ sec^2. 10 ns/div.

(b) Compressed Pulse Envelope, 10 ns/div.

(c) Compressed Pulse Envelope, 1 ns/div.

pression was observed was approximately 3×10^{16} cycles/sec.^{2}, fifty percent higher than anticipated. Aside from a point-by-point phase measurement, Figure 10, no attempt was made to establish the reason for the discrepancy. One approximation made in the calculations which could explain part of the difference is the assumption that the meander line is completely immersed in dielectric. Some coupling will take place in the air gaps between adjacent turns of the meander, and any warpage existing in the top dielectric sheet would allow coupling through air. For example, if sufficient coupling takes place in air to reduce the effective velocity constant $\sqrt{\epsilon_r}$ to 1.390 from the assumed value of 1.665, the differential delay will be reduced from 50 ns. to 33 ns. which would match the filter to a scan rate of 3×10^{16} cycles/sec^2.

Figure 9a shows the detected envelope of the uncompressed pulse scanning at approximately 3×10^{16} cycles/sec^2. The compressed pulse, Figures 9b and 9c, has a peak-to-sidelobe ratio of 11 db. The uncompressed pulse was adjusted to have approximately the same noise level as the compressed pulse for these photographs, this requiring a 13 db attenuator to be inserted in place of the filter.

The compression characteristic of the filter is sensitive to scan rate errors, an error of two percent being sufficient to reduce the compressed pulse to the level of the sidelobes.

The phase characteristic as measured with the phase bridge, Figure 1, agrees with the delay slope determined by the compression measurement. Figure 10 is a graph of measured phase vs frequency with a constant phase added to reference the plot to zero. The error curve at the bottom of Figure 10 is the difference between the measured phase ϕ_m and a true quadratic phase ϕ_c, matched to the measured values at 1.2 and 1.8 Gc. A curve which closely matches the measured one is

$$\phi_c = 15.67\, f^2, \quad f \text{ in Gc} \tag{2.14}$$

For a linear scan,

$$f = f_0 + St \tag{2.15}$$

The corresponding phase function is

$$\phi = \int f\,dt = f_0 t + \frac{1}{2} S t^2 + \phi_0 \tag{2.16}$$

where

ϕ = phase of scanning signal in cycles

f_0 = frequency at t = 0.

$\phi_0 = \phi$ when t = 0.

Combining Eqs. (2.15) and (2.16)

$$\phi = \frac{1}{2S}(f^2 - f_0^2) + \phi_0 \tag{2.17}$$

Setting $\phi_c = \phi$, the scan rate which nearly matches the filter phase characteristic is found to be $S = 3.19 \times 10^{16}$ cycles/sec^2.

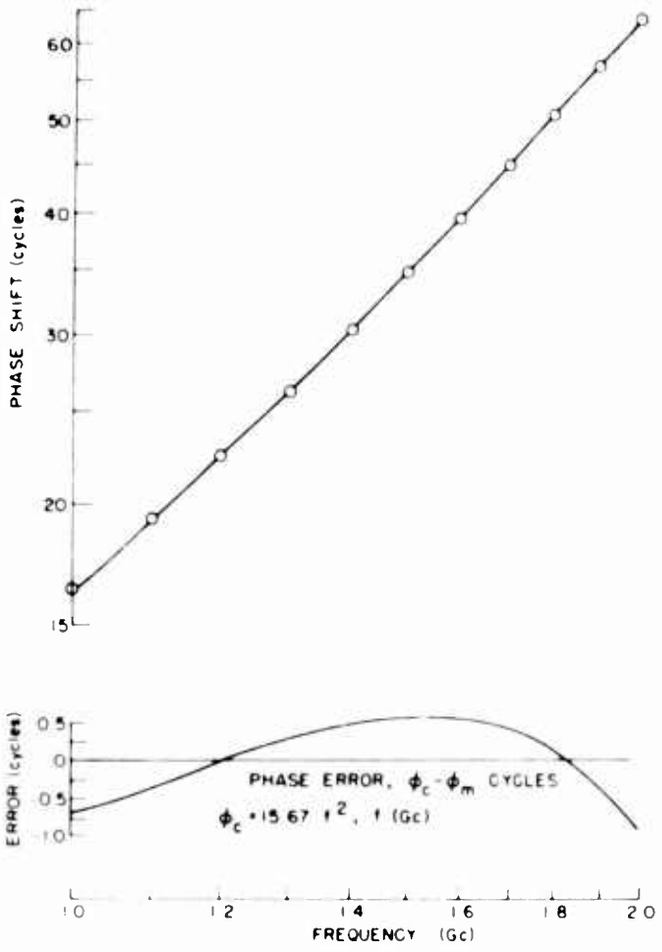

Figure 10. Measured Phase vs Frequency, PCML

The phase error is almost one cycle at the ends of the range of measurement. Due to the fact that the effective bandwidth of the filter is centered near the low frequency end of the band, the actual phase error within the filter passband is probably much smaller than one cycle. The linearity of the error curve between 1.0 and 1.4 Gc indicates that a better match could be found for this frequency range. As a rough estimate, a straight-edge applied to the phase curve between 1.0 and 1.4 Gc can be made to match the curve within 0.2 cycles over this frequency range.

The input VSWR to PCML no. 2 is shown in Figure 11. The effectiveness of the relatively short (compared to a wavelength) transformer sections is indicated by the reasonably low reflections.

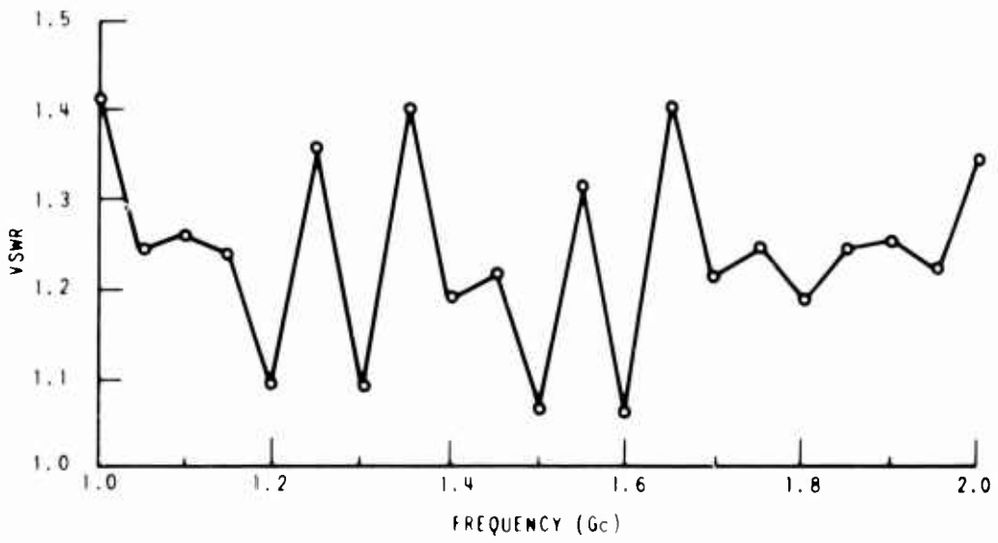

Figure 11. Input VSWR vs Frequency, PCML, B = 0.02 in.

E. CONCLUSION

The PCML investigation has accomplished its objective in establishing the usefulness of the meander line as a compression device. The

discrepancy between predicted and measured performance indicates that a more careful analysis would be in order before designing a filter for a specific application.

It appears that an attempt to realize octave bandwidths with a single-section PCML will result in minimum phase errors of approximately 1 cycle in a linear compression filter application. An approach employed by Dunn, Reference 21, in a similar structure is to cascade sections with different phase characteristics to approximate the desired curve. This could be carried to the point of having each turn of the meander different resulting in a tapered meander line.

A drawback of the PCML is the insertion loss associated with increasing delay. This loss can be compensated with a suitable network, but the total insertion loss would then be large.

As a result of this limited investigation, it appears that the PCML is a useful device for use as a compression filter of small-time-bandwidth product ($\Delta tb \simeq 10$). As compared with the other techniques investigated under this contract, the advantages of the PCML include:

1. It is physically compact
2. It is dimensionally stable
3. It can be easily reproduced by photo-etching

Disadvantages include:

1. The filter cannot easily be adjusted.
2. It is sensitive to scan rate errors.
3. It has high insertion loss for large delays.

III. THE TAPPED DELAY LINE

A. DESCRIPTION

The Tapped Delay Line (TDL) approach to compression filter design involves a series of bandpass filters placed at approximately equal intervals along a delay line. The pass-bands of the filters are centered at different frequencies such that the average delay characteristic of the structure is linearly dispersive. The composite bandwidth of the filters will be the compression bandwidth as illustrated by Figure 12.

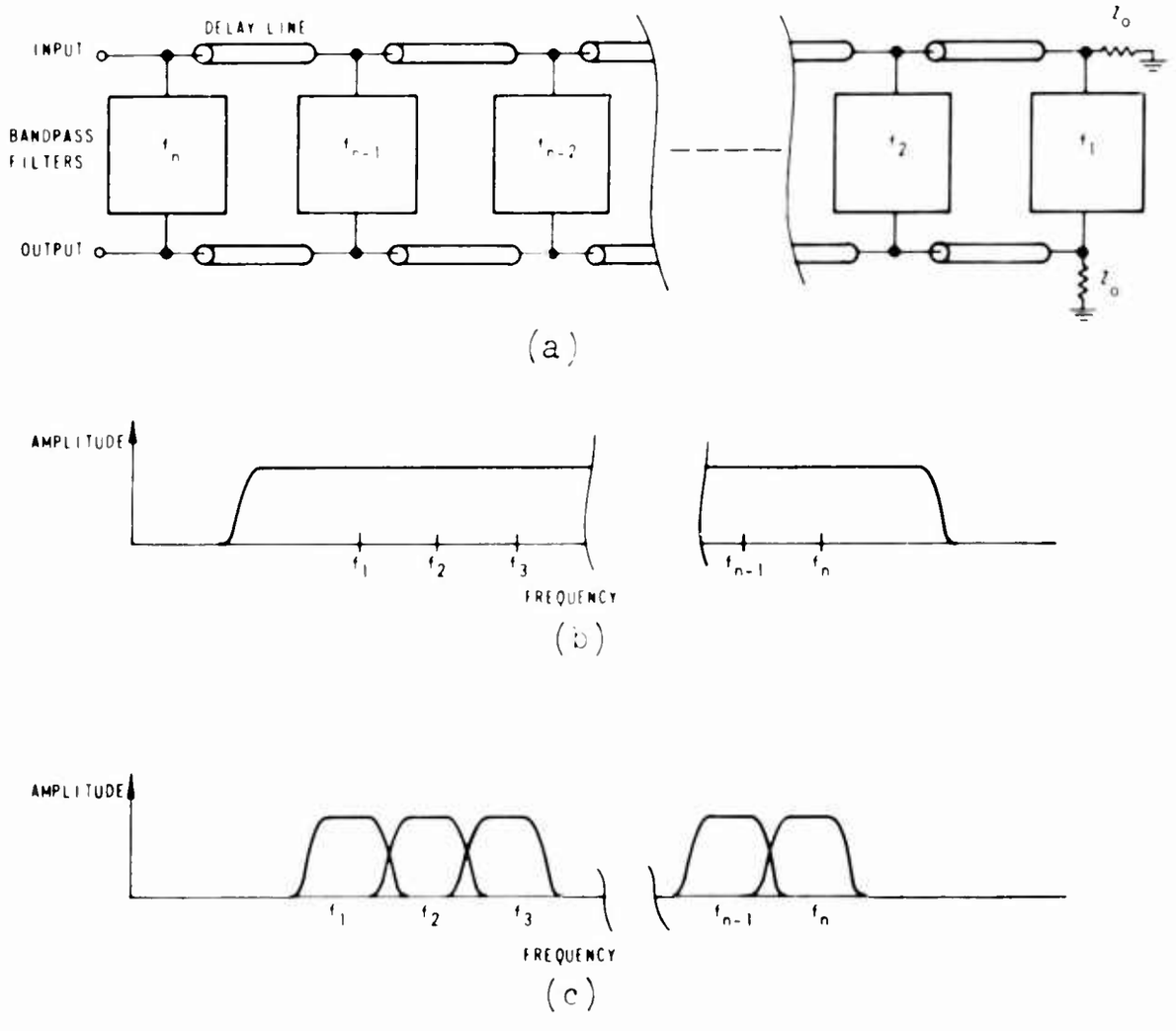

Figure 12. TDL Schematic Diagram
(a) TDL with n Filters
(b) Idealized Frequency Spectrum of Input Signal
(c) Idealized Spectrum of response of Compression Filter to Rectangular Input Signal.

Compression is accomplished by adjusting the delays between filters so that the response envelopes of the individual filters are superimposed when a scanning input signal of the proper scan rate is applied. This is illustrated for two filters in Figure 13. A means of fine adjustment of delay between filters is necessary to cause phase addition at one instant in time for all the bandpass filters simultaneously. (Figure 14). This is analogous in many respects to the radiation pattern of an antenna array where each element of the antenna is excited by a different frequency. The distant radiation pattern will then exhibit a major peak at each point where contributions from all elements add in phase. Thus an analog relationship exists between radial distance (in the plane of the antenna array) and time. Similarly, an analog relationship exists between the directivity pattern of each element of the array and the bandpass shape of the individual filters of a TDL.

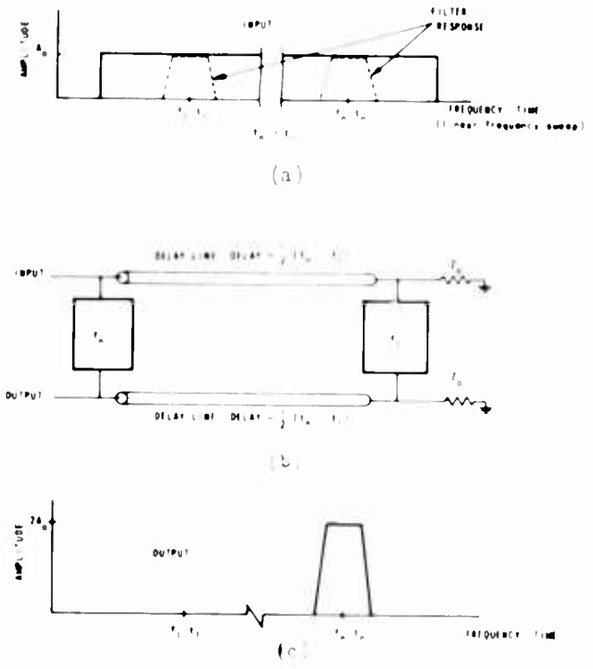

Figure 13. Time Relationships in an n - Filter Tapped Delay Line Compression System Showing only First and Last Filters.
(a) Input Signal Spectrum with Filter Passbands Superimposed.
(b) Tapped Delay Line
(c) Compression Filter Output Showing Superimposed Envelopes of two Filter Passbands.

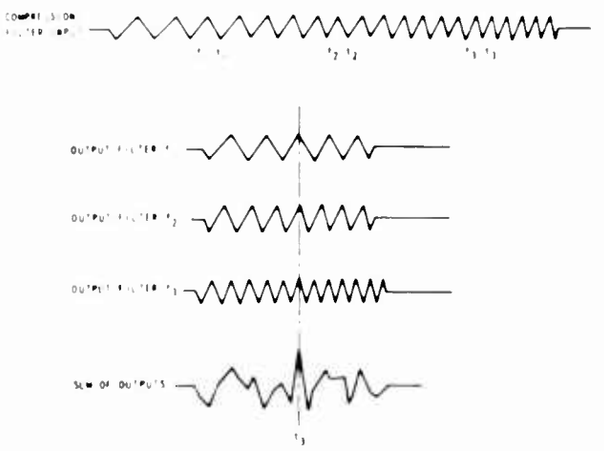

Figure 14. Tapped Delay Line Compression Filter with Three Elements. The scanning input signal is divided into three sections by the three bandpass filters. The filter outputs are combined at the output of the compression filter to cause a major peak to appear at t_3.

The response of the TDL will consist of several major peaks similar to those of the antenna array. By increasing the number of filters, the peaks can be moved further apart in time just as adding more elements to an antenna array increases the distance between major lobes. The undesired major peaks will be suppressed to the extent that they are caused by the in-phase condition of frequencies which fall outside the filter pass-band.

It is desirable in this configuration then, to use as many filters as possible in the TDL. This number is limited to the ratio of the desired TDL bandwidth to the individual filter bandwidth. In the case under consideration, the desired TDL bandwidth is 1 Gc and the smallest filter bandwidth compatible with the 2×10^{16} cycles/sec^2 scan rate is approximately 100 Mc. Thus, ten filters are required.

The filter bandwidth which provides the minimum response duration to a scanning excitation is given approximately by *

---

* The response of a bandpass filter is discussed in References 3 and 10, among others. Eq. (3.1) is taken from Reference 3 where it appears as: $b_{opt} = \sqrt{KS}$ where K is the product of the bandwidth and risetime of the filter.

$$\Delta f \cong \sqrt{\frac{S}{2}} \qquad (3.1)$$

Δf is the half-power bandwidth in cps

S is scan rate in cycles/sec^2

This equation requires a bandwidth of approximately 100 Mc for a scan rate of 2×10^{16} cycles/sec^2

B. FILTER DESIGN

For a total compression bandwidth of 1 Gc, ten 100 Mc filters are required. These will extract almost all the available signal energy if the filters are spaced so that 3 db points coincide on adjacent filters. To cover the range from 1 to 2 Gc, ten filters with center frequencies of 1050, 1150, ------, 1850, 1950 Mc are required.

The design parameters for the filters is taken from two reports*

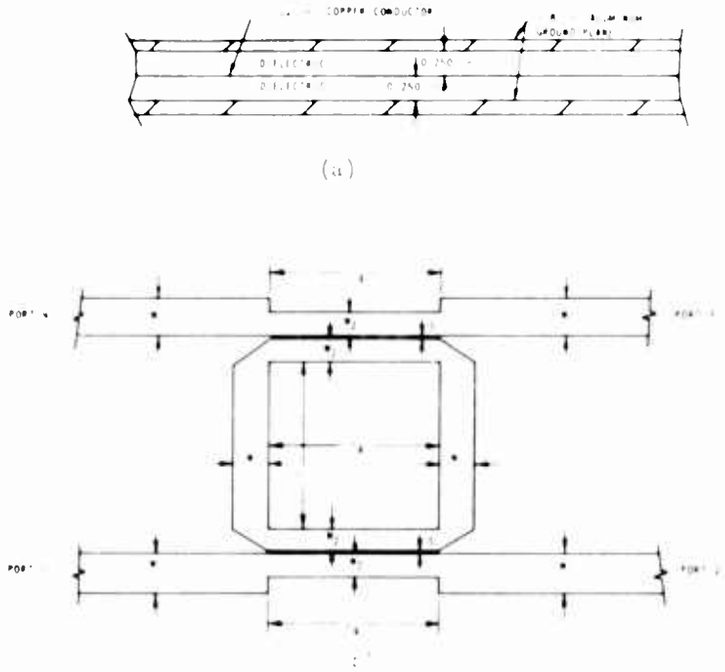

Figure 15. Strip-Line Resonant-Loop Bandpass Filter.
(a) Edge View of strip-line structure. The copper tape is enclosed between two polystyrene dielectric sheets by aluminum ground planes.
(b) Top view of filter as seen with one ground plane removed.

---

* References 11 and 12

describing strip transmission lines and microwave components. Figure 15 illustrates the configuration of a 100 Mc. bandpass filter. This is representative of all filters in the system.

The filter is electrically similar to a pair of directional couplers except that due to the recirculating wave on the loop, coupling at loop resonance is tighter than it would be with a paired directional coupler. The center frequency of the filter is the frequency at which the electrical distance around the loop is one wavelength and the length of the coupling gap, L, is one quarter wavelength. At this frequency, the signal entering port 1 (Figure 15) excites a wave traveling in a clockwise direction on the loop. This wave couples out into port 4, ports 2 and 3 being isolated. At some frequency different from the center frequency, some portion of the energy couples into port 4, the remainder emerging at port 2 while port 3 remains isolated. This is illustrated graphically in Figure 16.

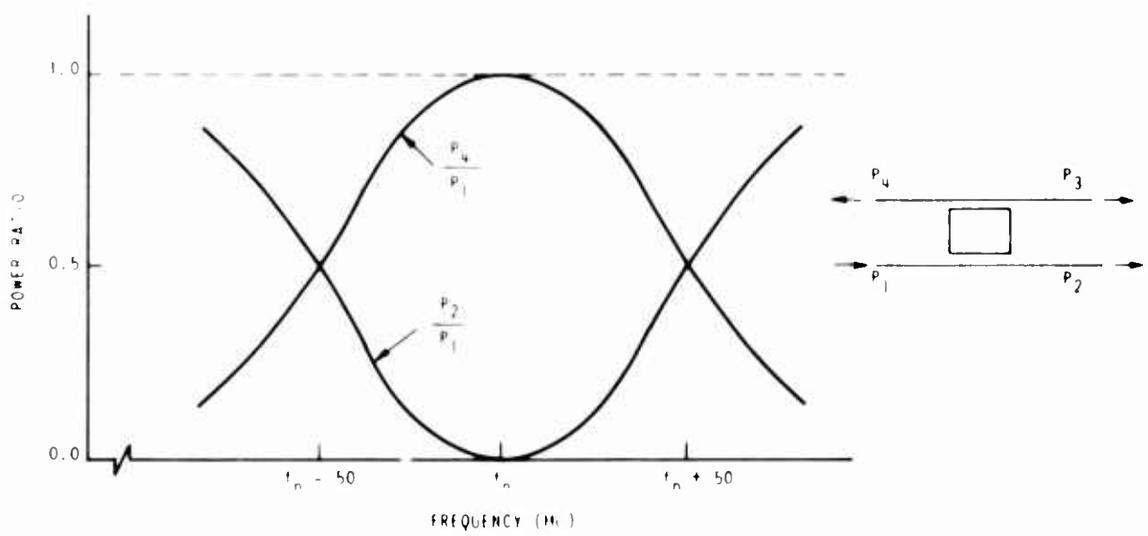

Figure 16 Resonant loop Filter Coupling Diagram.
Filter Bandwidth = 100 Mc.

Each port is connected to a strip-line to Type N coaxial adapter to match the delay cable Type N connectors. The adapters and other strip-

line components make use of conventional techniques*, hence only the filters will be described in detail.

The dimensions of the strip outside of the coupling region (dimension ω_1, in Figure 15) are obtained from Figures 2-3, References 12. For Z_0 = 50 ohms, strip thickness = 0.0022 in., 0.505 in. ground plane spacing and polystyrene dielectric with $\sqrt{\epsilon_r} = 1.6$, the strip width is found to be 0.375 inches.

The dimensions of the strip within the coupling region ω_2, are obtained from two nomograms (Figures 16 and 17) in Reference 12. To use these nomograms, it is necessary to know the even and odd mode coupled line impedances Z_{oe} and Z_{oo}. These are the impedances of one section of a coupled strip to ground with equal currents in both strips in the same direction, and opposite directions, respectively. Combining equations (4.4) and (4.8) from Reference 12, the impedances are obtained as functions of the voltage coupling coefficient k.

$$Z_{oo} = Z_o \left(\frac{1-k}{1+k}\right)^{1/2} \tag{3.2}$$

$$Z_{oe} = Z_o \left(\frac{1+k}{1-k}\right)^{1/2} \tag{3.3}$$

The coupling coefficent is determined by the loaded Q of the filter as given by Eq. (5 13), Reference 11:

$$Q = \frac{n\pi(1-c_1^2)^{1/2}\exp\left(-\frac{\alpha D}{2}\right)}{1-(1-c_1^2)\exp(-\alpha D)} \tag{3.4}$$

n = 1 for single-tuned circuit

$c_1 = k$ for single-tuned circuit

α = loss coefficient and is approximately zero

D is the free-space wavelength of the loop.

---

* References 12 and 13 are useful design manuals for strip-line components. Reference 13 is a handbook which contains many curves describing strip-line component performance. The strip-line to coaxial transition is illustrated in Figure 3-3, Reference 13.

Substituting $n = 1$, $c_l = k$, and $\alpha = o$ in Eq. (3.4) and solving for k,

$$k \cong \left[-\frac{B^2\pi^2}{2} \pm B\pi \left(\frac{B^2\pi^2}{4} + 1 \right)^{1/2} \right] \tag{3.5}$$

$$B \triangleq \frac{1}{Q} = \frac{\Delta f}{f_o} \tag{3.6}$$

Δf is half-power bandwidth

f_n is filter center frequency

Figure 17 is a tabulation of the design parameters of the ten filters as obtained by Equations (3.2) through (3.6). The inside dimensions of the loop are L and L'. L is one-quarter wavelength in the dielectric, and for polystyrene,

$$L = \frac{7.382}{f_o \times 10^{-9}} \quad \text{inches} \tag{3.7}$$

L' is empirically found to be given by the expression

$$L' = L - \frac{f_n \times 10^{-9}}{4.0} + 0.187 \text{ inches} \tag{3.8}$$

f_n MC	B	K	Z_{oo} ohms	Z_{oe} ohms	ω_2 inches	S inches	L inches	L' inches
1050	0.0952	0.507	28.6	87.3	0.228	0.0040	1.785	1.683
1150	0.0869	0.492	29.2	85.6	0.238	0.0048	1.605	1.505
1250	0.0800	0.471	30.0	83.4	0.242	0.0061	1.475	1.355
1350	0.0741	0.455	30.6	81.6	0.250	0.0071	1.368	1.223
1450	0.0690	0.440	31.2	80.0	0.258	0.0086	1.272	1.108
1550	0.0645	0.428	31.95	78.3	0.265	0.0101	1.191	0.996
1650	0.0606	0.415	32.2	77.6	0.270	0.0111	1.120	0.905
1750	0.0571	0.405	32.5	77.0	0.271	0.0116	1.055	0.810
1850	0.0540	0.395	32.9	76.0	0.273	0.0131	1.000	0.825
1950	0.0523	0.390	33.1	75.5	0.278	0.0139	0.946	0.647

Figure 17. Tabulation of TDL Filter Parameters. For all filters, $\Delta f = 100$ Mc, ground plane spacing is 0.505 in., $\sqrt{\epsilon_r} = 1.60$, strip thickness is 0.0022 in. All dimensional parameters are defined in Figure 19.

C. CONSTRUCTION

Each filter assembly consists of the copper conductors bonded to a 3 1/2 in. x 5 in. polystyrene dielectric sheet. The dielectric sheets are 0.250 in. thick, the conductor is 0.0022 in. copper, and the adhesive is a 0.003 in. layer of silicone*. The total distance between ground planes is 0.505 in.

Half the assembled structure is shown in Figure 18 with one of the ground planes removed. The other half is almost identical to this in appearance, the only differences being in the loop size and the amount of aquadag used. Figure 19 is a schematic of the completed filter.

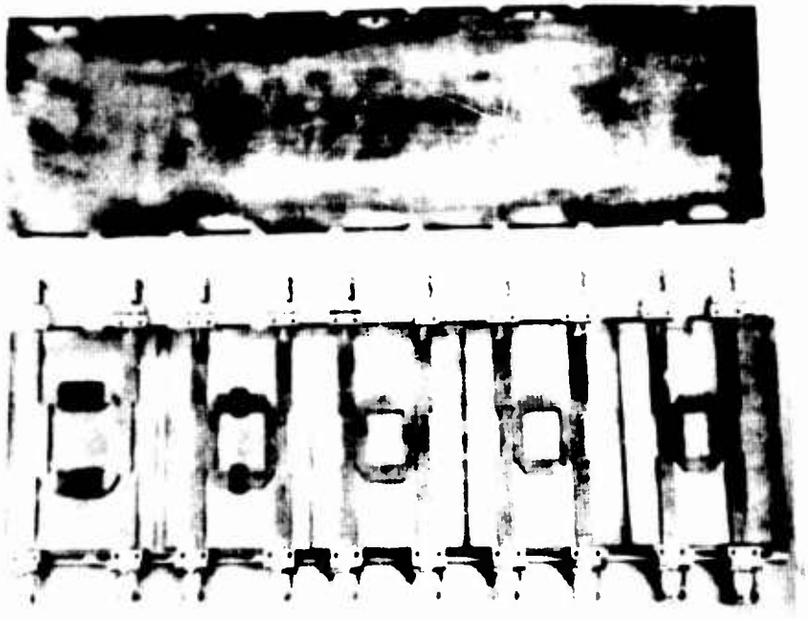

Figure 18. Photograph of Five of the Ten Sections of the TDL. Upper ground plane is shown beside filter. From left to right, the center frequencies are 1050, 1250, 1450, 1650, and 1850 Mc. Aquadag is applied to the two lowest frequency loops to equalize attenuation.

---

* The copper tape with the adhesive backing is marketed as No. 7420 "Mystic Tape" by Mystic Adhesive Products, Inc.

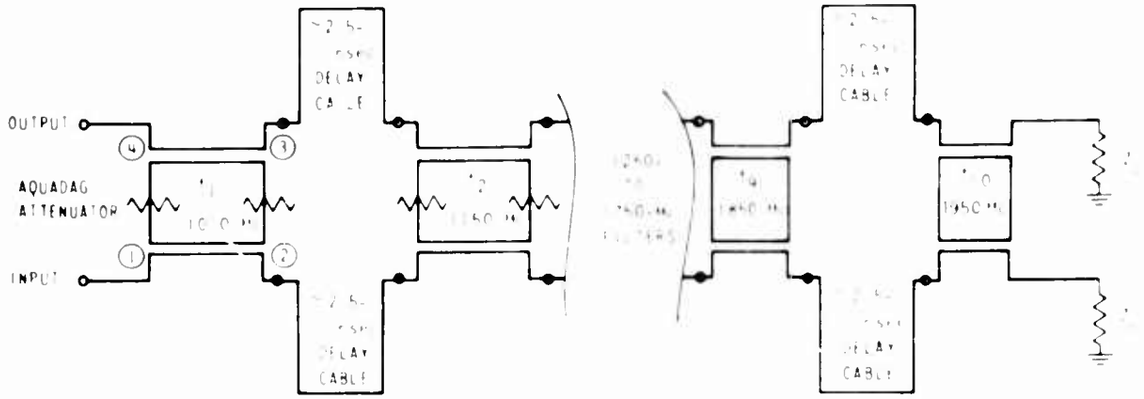

Figure 19. Schematic Diagram of TDL Showing Interconnections between Ports. Circled Numbers on the 1050 Mc Filters are Port Numbers, the Ports on the Other Filters being in the same relative Positions.

To construct a filter, a length of copper tape is bonded to the dielectric sheet and rolled flat to remove bubbles. The outline of the loop is then scribed into the copper with a fine point, this being followed with a sharp cutting tool such as a razor blade. Care should be taken to avoid rolling the copper into the cut, especially in the coupling gap where this can increase the coupling undesirably. The excess material is removed leaving the loop. The arms of the coupler can then be placed in position with a piece of shim stock or some other material of the proper thickness in the gap to assure the correct value of s. The cutouts in the arms should be made prior to placing the strip in place so that the gap is not disturbed.

The corners of the loops are mitered to reduce reflections at the corners. Figure 2.2 in Reference 13* indicates the reduction in VSWR to

---

* A strip line 90° bend with ground plane spacing of 0.500 in. and a conductor width of 0.400 in. is shown to have a VSWR of 2.4 at 3 Gc. Another plot snows that a 90° bend mitered as shown in Figure 20 (this report) will have a VSWR of approximately 1.05.

obtained with the mitered corners. The dashed lines in Figure 20 are extentions of the inner border of the loop and mark the points at which the corner is cut.

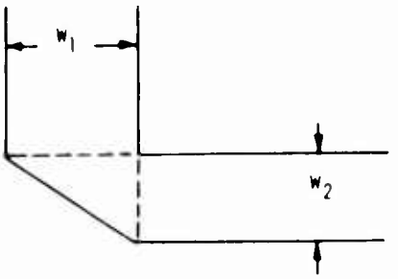

Figure 20. Method of Mitering the Corners of the Stripline Loop

D. PERFORMANCE

Figure 21 is typical of the frequency response of the ten filters in the TDL. The low loss between ports 1 and 2 and the isolation between ports 1 and 3 make possible the cascaded arrangement of Figure 19 with a maximum attenuation of 14 db through all ten filters and the 50 ns of delay cable at 2 Gc. The aquadag on the low frequency loops was used to compensate in part for the cable loss.

The compression performance of the TDL is illustrated by Figures 21, 22, and 23. The peak-to-sidelobe ratio as observed from Figure 22 is approximately 12 db with a half-power pulse width of about 1 ns. The effectiveness of the TDL in improving the signal-to-noise ratio is illustrated by Figure 23. The noise is surpressed by the attenuation of the filter while the signal is increased in amplitude.

Figure 24 shows how the TDL "spreads out" a signal sweeping in the wrong direction; in this case, from low to high frequency. The ratio of amplitudes of the response to signal and image is about 8 db.

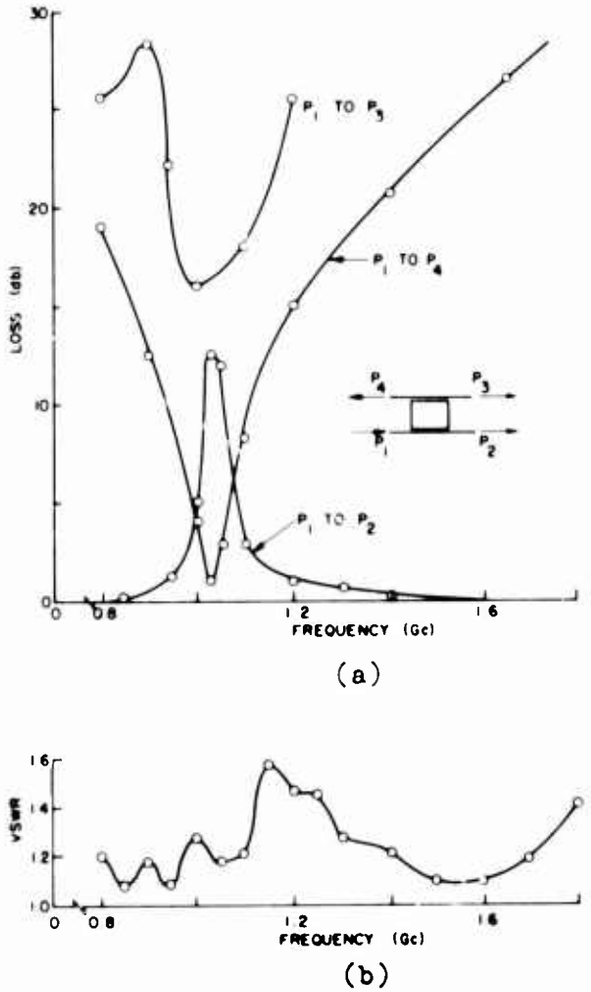

Figure 21. Insertion Characteristics and VSWR of 1050 Mc Filter
(a) Insertion Loss vs Frequency
(b) VSWR vs Frequency

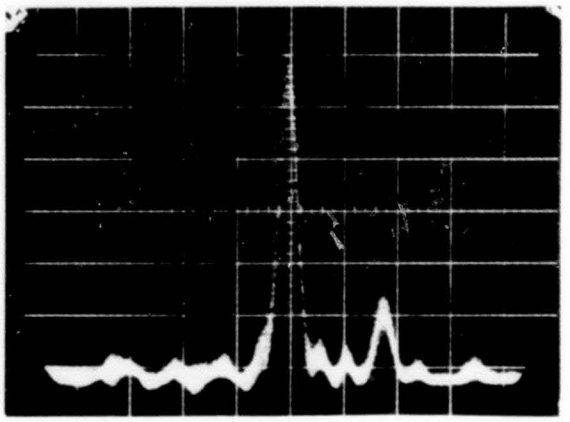

a. Time scale: 5 ns/div.

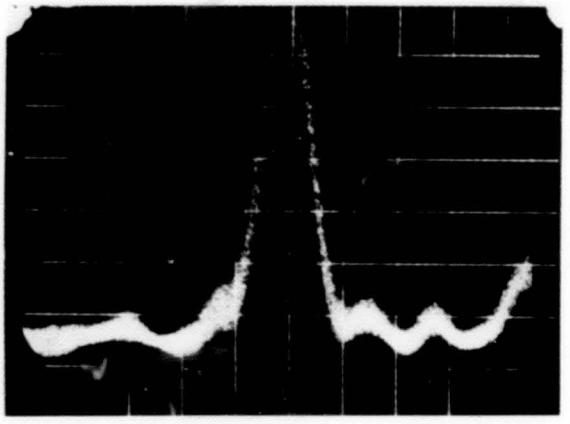

b. Time scale: 1 ns/div.

Figure 22. Compressed Output Pulse, TDL.
$S = 2 \times 10^{16}$ cycles/sec^2. Amplitude scale is approximately linear.
a. Time scale: 5 ns/div.
b. Time scale: 1 ns/div.

a. Noise input to TDL.

b. Signal + Noise at input to TDL.

c. Signal + Noise at output of TDL.

Figure 23. Performance of TDL in presence of Noise - (5 ns/div.)
a, b, and c are same relative amplitude scales.
a. Noise imput to TDL.
b. Signal + Noise at input to TDL.
c. Signal + Noise at output of TDL.

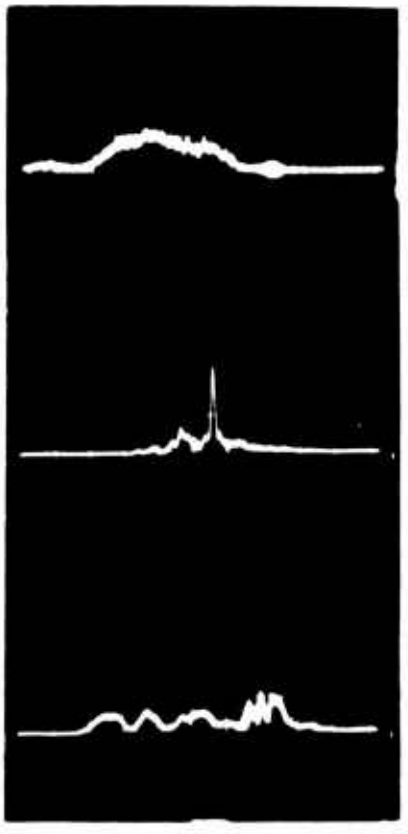

a. Downsweeping (Frequency decreasing with time) input to TDL

b. Compressed response to a.

c. Response to an upsweeping signal in same time position as a. (Image Response)

Figure 24. Signal and Image Response of TDL.
a, b, and c are at 10 ns/div. and have same relative time scales.
a. Downsweeping (Frequency decreasing with time) input to TDL
b. Compressed response to a.
c. Response to an upsweeping signal in same time position as a. (Image Response)

E. AN IMPROVED MODEL

In an attempt to reduce the volume and weight of the package and at the same time to provide an easier method of adjusting phase, the TDL was redesigned with the following changes:

1. The ground plane spacing was reduced to 0.251 in. from 0.505 in.
2. Tellite 3B clad with 0.001 in. copper was used as the dielectric material instead of Polystyrene.
3. The filters were photo-etched instead of being cut from stock.
4. The delay lines were photo-etched strip line instead of RG - 9/U cable.
5. Sliding trombone-type line stretchers were employed between filters as a means of phase adjustment.

The construction of the filter is illustrated in Figures 25 through 27. The four layer TDL illustrated is composed of stacked sections, each consisting of a bandpass filter and adjustable delay line section. Figure 25 shows the construction of one of the layers. The piece of dielectric with the two "U" shaped sections of conductor is the sliding portion of the delay line and can be adjusted to change the delay between adjacent filters by ± 0.42 ns.

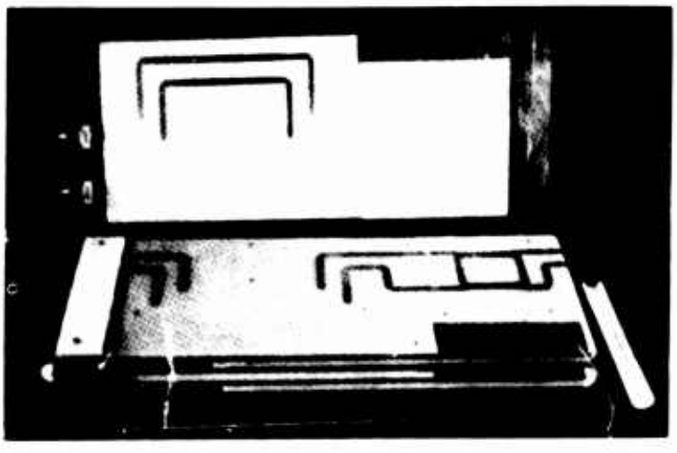

Figure 25. Photo-Etched TDL with Four Sections: f_o = 0.95, 1.05, 1.15 and 1.25 Gc.

The strip-line transition between layers of the filter is shown in Figures 26 and 27. This method was chosen in preference to other methods because it is relatively simple to construct and involves no sudden changes in E-M field configuration. The use of 0.125 in. dielectric sheets and ground planes allows standard size brass and teflon tubing to be used in the construction of the transitions.

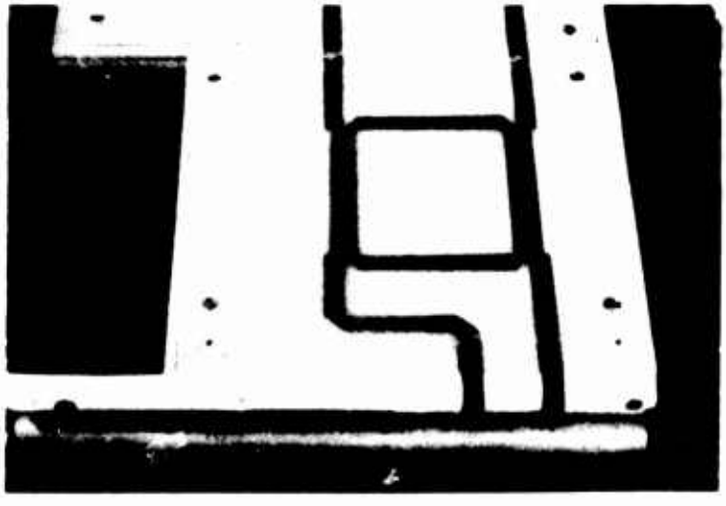

Figure 26. Close-up Photograph of Photo-Etched TDL Showing Details of 1.25 Gc. Filter and Strip-Line Transition Between Layers.

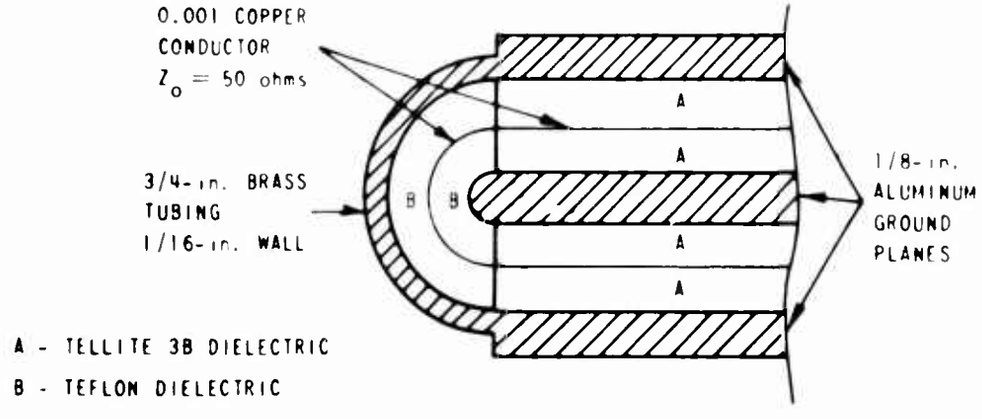

Figure 27. Edge View of Transition Between Layers

The filter parameters are calculated in the same way as for the original TDL. Figure 28 is a table of filter parameters which are re-calculated for the photo-etched TDL. Equation 3.8 was found to be inaccurate when used with the decreased ground plane spacing and different dielectric, and a new equation was formulated from measurements on prototype filters. The empirical equation for L' is

$$L' = L - 0.150 - 0.025 \frac{f_o - 1050}{100} \text{ in.} \tag{3.9}$$

f_o = filter center frequency in Mc.

This equation was formulated from measurements on two filters for which F_o = 1010 and 1250 Mc. No filters have been constructed for f_o higher than 1250Mc so the accuracy of Eq. (3.9) is not known for the higher frequencies.

f_o Mc	$\sqrt{\epsilon_r} Z_{oo}$ ohms	$\sqrt{\epsilon_r} Z_{oe}$ ohms	ω_2 ins.	s ins.	L ins.	L' ins.
950	42.3	137	0.118	0.0013	2.040	1.915
1050	43.5	133	0.123	0.0016	1.845	1.695
1150	44.6	130	0.125	0.0020	1.685	1.510
1250	45.7	127	0.130	0.0025	1.550	1.350
1350	46.6	127	0.134	0.0027	1.435	1.210
1450	47.4	122	0.137	0.0033	1.335	1.085
1550	48.2	120	0.140	0.0040	1.250	0.975
1650	48.9	119	0.142	0.0048	1.173	0.873
1750	49.5	117	0.144	0.0050	1.106	0.781
1850	50.1	115	0.146	0.0055	1.048	0.698

Figure 28. Tabulation of Photo-Etched TML Dimensions. f = 100 Mc, Ground Plane Spacing is 0.251 in., strip thickness is 0.001 in., ω = 0.184 in. for Zo = 50 Ω.

The response of a single filter (f_o = 1010 Mc) to a scanning input is shown in Figure 29. This illustrates the "beat" which results from the natural response of the filter being added to the scanning excitation signal. A similar phenomenon is observed in Reference 10 in an analog computer study of the response of a bandpass filter to a scanning excitation.

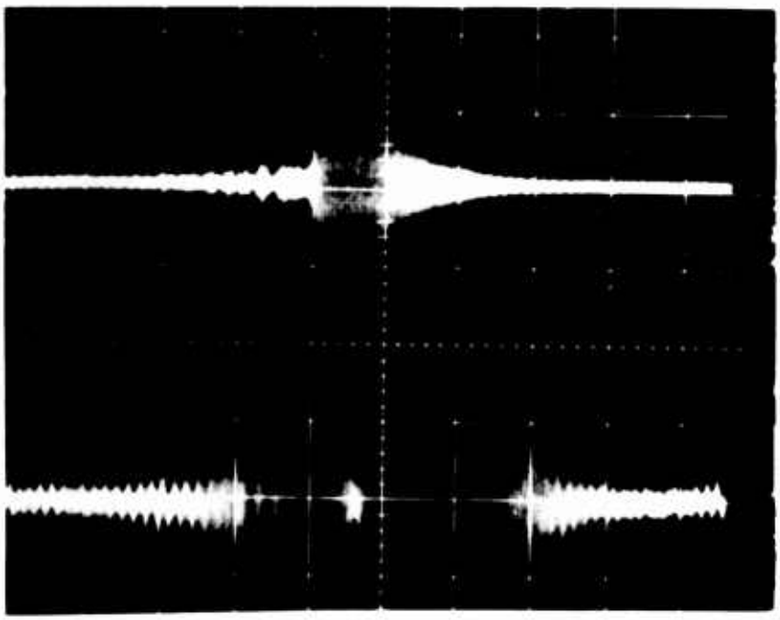

Figure 29. Response of Single Filter Section to Scanning Input ($S = 2 \times 10^{16}$ cycles/sec^2) Input is applied to Port 1, frequency is decreasing from left to right. CRO bandwidth = 1 Gc

Top trace: response at port 2 showing portion of signal energy removed.
Bottom trace: response at port 4 showing filter passband, same time relationship as upper trace.

The response of the four-section TML to the same scanning excitation as Figure 29 is shown in Figure 30. The peak-to-sidelobe ratio is approximately 13 db with a half-power pulse-width of about 2 ns. The larger width is a result of the bandwidth of the filter being less than the full ten section filter tested previously.

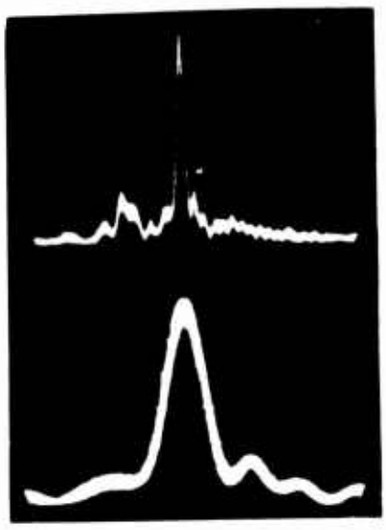

(a. 5 nx/div.

(b. 2 ns/div.

Figure 30. Response of Four-Section Filter to Scanning Signal ($S = 2 \times 10^{16}$ cycles/sec^2) Response Envelope amplitude is proportional to power.

The four sections constructed adequately proved the usefulness of the photo-etching technique. In addition to the compactness of the structure and the ability of the filter to be quickly adjusted to any scan rate within its range of adjustment (approximately 1.84×10^{16} to 2.17×10^{16} cycles/sec^2), the filter can be matched to upsweeping as well as downsweeping signals. In view of the expense involved in etching the filters to the required tolerances, it was decided not to complete the full ten section filter as the primary objective of the investigation had been met in establishing the usefulness of the technique.

F. CONCLUSIONS

The TDL has been shown to provide compression and to have certain desirable characteristics. These are:

1. The TDL can be matched to various scan rates, within limits, without redesign of the structure.
2. The structure can be subjected to mechanical stress without affecting the electrical properties.

3. Upsweeping as well as downsweeping signals can be accommodated.
4. The overall attenuation characteristic of the TDL can be adjusted by introducing loss (aquadag coating) into the resonant filter elements.
5. The technique can be used to provide large time-bandwidth products, physical size being the primary limiting factor.
6. The insertion loss is relatively low.

Some undesirable characteristics are:

1. Relatively large physically.
2. Requires precision construction techniques.
3. Electrical properties are sensitive to temperature changes.

The compression characteristics appear to be comparable to other filter types investigated under this contract. It is possible that the use of a dispersive filter of small time-bandwidth product (such as PCML) at the output of each bandpass filter would provide superior performance to any of the filters tested. This would be a logical sequel investigation to the one covered in this report.

IV. THE TAPERED MEANDER LINE

A. PRINCIPLE OF OPERATION

It has been observed that a folded transmission line such as that shown in Figure 31 will radiate when the length of one of the parallel strips is equal to or greater than approximately one-half wavelength. The direction of radiation is normal to the plane of the meander, the directivity being related to the coarseness of the meander and the taper of the line. If two meander lines with similar tapers are operated parallel to each other as shown in Figure 31b, coupling will take place between a radiating element and the corresponding element on the parallel line.

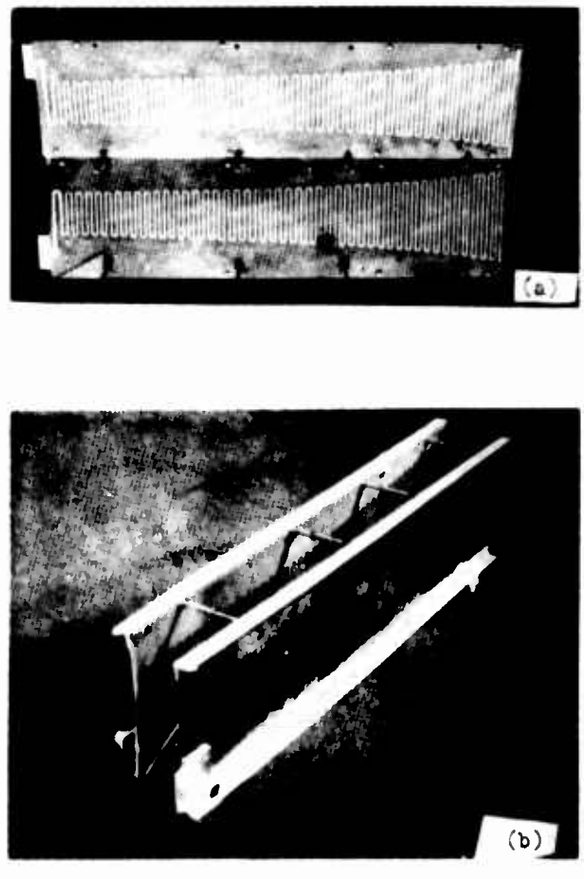

Figure 31. TML Compression Filter
(a) Meander line pair Showing Radiating Surfaces
(b) Meander Line Pair in Operating Position

The frequency-selective coupling can be used to compress a scanning signal by adjusting the taper to give the desired delay characteristics. The TML technique appears to be useful only for compressing upsweeping signals as no compression has been obtained by us for a signal which sweeps down in frequency.

The directivity of the radiation is shown by the experimental result in Figure 32b. The point of maximum coupling between the meander line and the antenna is directly opposite the point for which $2(M + N) = \lambda$. The

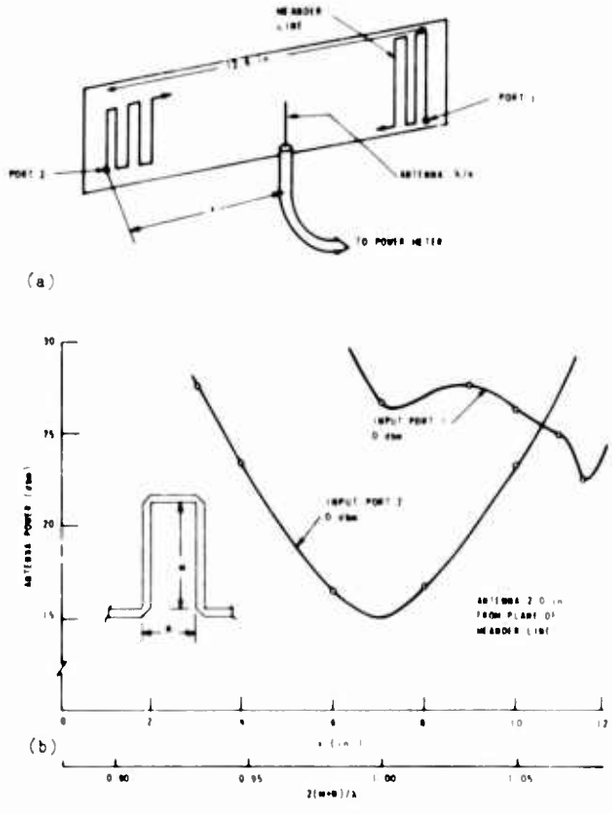

Figure 32. TML Radiation Pattern
(a) Radiation Pattern Measurement
(b) Power Received By Antenna Vs Distance Along Line and Normalized Wavelength

curve of Figure 32b is repeatable for any λ within range of the TML. The group delay of a signal applied at the high-frequency end of the line (Port 2 in Figure 32a) is twice the delay of the meander up to the point of radiation plus the delay of the air gap between the conjugate meander lines.

The delayed signal emerges from the receiving meander line at the port opposite the input port.

A signal applied to Port 1 (the low frequency end) does not exhibit an easily predictable delay characteristic due to non-selective radiation from portions of the meander line for which $< \lambda$. This is illustrated in Figure 32b by the Port 1 line which indicates that signal energy is radiated by all portions of the line for which the period (M + N) is greater than one wavelength. For this reason, a downsweeping TML does not appear practical.

B. DESIGN AND CONSTRUCTION

The TML described here was designed to have the same parameters as the other types of filters described previously. That is, the filter design bandwidth is 1 Gc and optimum compression is to be obtained at a scan rate of 2×10^{16} cycles/sec^2. The completed filter is shown in Figures 31 and 31. In the first figure, the two sections are placed together in such a way that the meanders can both be seen. It should be noted that one of the meanders is a mirror-image of the other. As the conductors were photo-etched on the dielectric, the line and its image were easily formed by exposing the sensitized copper through opposite sides of the negative.

The Type-N to stripline connector is mounted on the narrow end of the line (port B in Figure 32a), the other end being terminated in a metallized film resistor. The first two turns of the meander are tapered to provide an impedance transformation from 50 ohms to the line impedance, approximately 75 ohms. This shown in Figure 31.

In rder to maximize frequency-delay selectivity, it was desirable to use as many turns as possible in the meander. This was accomplished by using the single-strip above ground plane (Microstrip) construction technique and by increasing the b dimension (Figure 32b) until no coupling was observed between adjacent turns. The Microstrip configuration confines

the E-M fields so that a relatively small b can be used. By allowing very little coupling between turns, the propagation velocity is maintained at essentially $c / \sqrt{\epsilon_r}$ which allows a large number of turns for a given delay. As was shown in the case of the PCML, coupling between adjacent turns has the effect of slowing the group velocity. This would appear to be undesirable in the TML due to the decreased number of turns for a given delay (causing increased ripple in the phase shift vs frequency curve) and because of the increased attenuation encountered when coupling occurs between turns.

The method used in calculating filter dimensions was to make each of the parallel turns of the meander the appropriate length (dimension a, Figure 32b) for the total delay of the meander up to that point. As an example, a filter is to be designed to compress a signal in the frequency range f_2 to f_1 where $f_1 < f_2 \leq f_1$. The scan rate is S, and the delay required for a given frequency f is

$$\tau_f = \Delta\tau\left(\frac{f - f_1}{f_2 - f_1}\right) \tag{4.1}$$

where for an upsweeping signal

$$\Delta\tau = \frac{f_2 - f_1}{S} \tag{4.2}$$

The delay from the input to the n^{th} radiating element of the meander line is

$$\tau_n = \frac{\sqrt{\epsilon_r}}{c} \sum_{i=2}^{n} (A_{i-1} + b_{i-1}), \quad i > 1$$
$$\tau_n \triangleq 0 \text{ for } i = 1 \tag{4.3}$$

where $\frac{c}{\sqrt{\epsilon_r}}$ is the propagation velocity on the meander line, and a, b are dimensions of the line. Figure 33. Equation (33) defines the input to the filter as the beginning of the first radiating element. Since we are only concerned with the differential delay, it is reasonable to define delay as being relative to the input to the delay-varying elements.

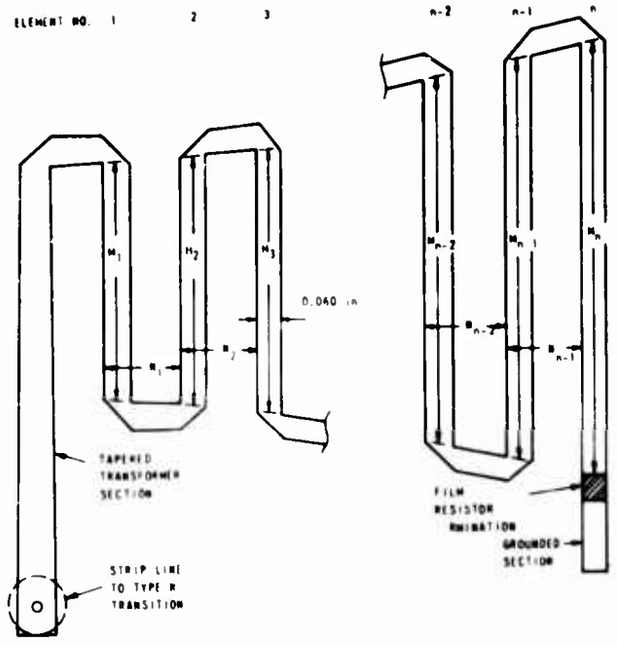

Figure 33. Tapered Meander Line Dimensions

The frequency to be radiated from the n^{th} element is found by setting $\tau_f = 2\tau_n$ since the signal of frequency f has to traverse two meander lines from input to output. Knowing the frequency of the n^{th} element, and having established a value for $N = N_1 = N_2 \ldots\ldots = N_n$, M_n is found from the following relation:

$$M_n = \frac{\lambda}{2} - M_n = \frac{c}{2\sqrt{\epsilon_r}\, f} - N \qquad (4.4)$$

The TML of Figure 31 was constructed in the manner just described with the following parameters:

$f_2 = 2.0$ Gc.

$f_1 = 1.0$ Gc.

$S = 2 \times 10^{16}$ cycles/sec^2

$N = 0.200$ in.

$\sqrt{\epsilon_r} = 1.52$ (Tellite 3B dielectric)

The meander was photo-etched on the two sheets of Tellite using conventional techniques. The dielectric sheets were 1/16in. thick and had one oz. copper bonded to both sides. The meander was etched into one side of

each sheet, leaving the copper intact on the other side to serve as a ground plane.

The two meander lines were assembled as shown in Figure 31b. The 1/2 inch aluminum channels at the borders are for stiffening the structure, and the long screws allow adjustment of the spacing between the lines. The lines in the figure are spread further apart than normal in order to show more detail.

C. PERFORMANCE

The attenuation vs. frequency characteristic of the TML can be adjusted to a small degree by varying the distance between the two halves of the filter. Further frequency selective adjustment can be made by inserting lossy material in the space between the elements at the proper position. Figure 34 is a plot of the insertion loss of the TML with a

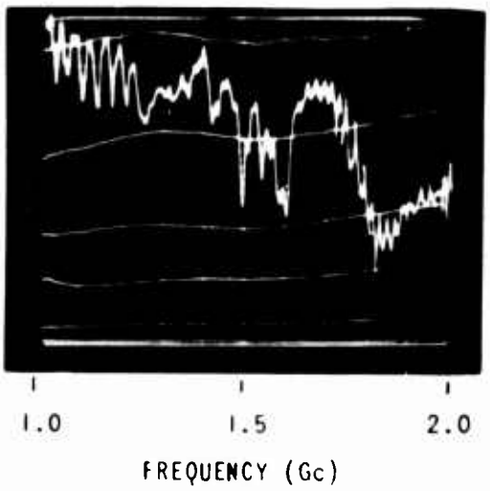

Figure 34. TML Insertion Loss vs Frequency. Horizontal Calibration Lines Represent 3, 6, 9, and 12 db respectively From top.

spacing of 0.50 inch between elements at the low frequency end and 0.85 in. at the high frequency end. This spacing was a compromise between lower overall loss with greater peak-to-peak variations and a higher

average loss with smaller variations. This spacing, incidentally, provided the greatest peak-to-sidelobe ratio of the compressed pulse.

Figures 35 and 36 show the response of the TML to a scanning signal, $S = 2 \times 10^{16}$ cycles/sec^2. As seen from Figure 35, the TML can provide a net compression gain of approximately 7 db. The next figure shows the peak-to-sidelobe ratio to be about 15 db with a half-power pulse width of less than 1 ns.

The sensitivity of the TML to scan rate errors is less than that of the PCML, the TML being able to tolerate almost a 10% error before reaching a peak-to-sidelobe ratio of unity.

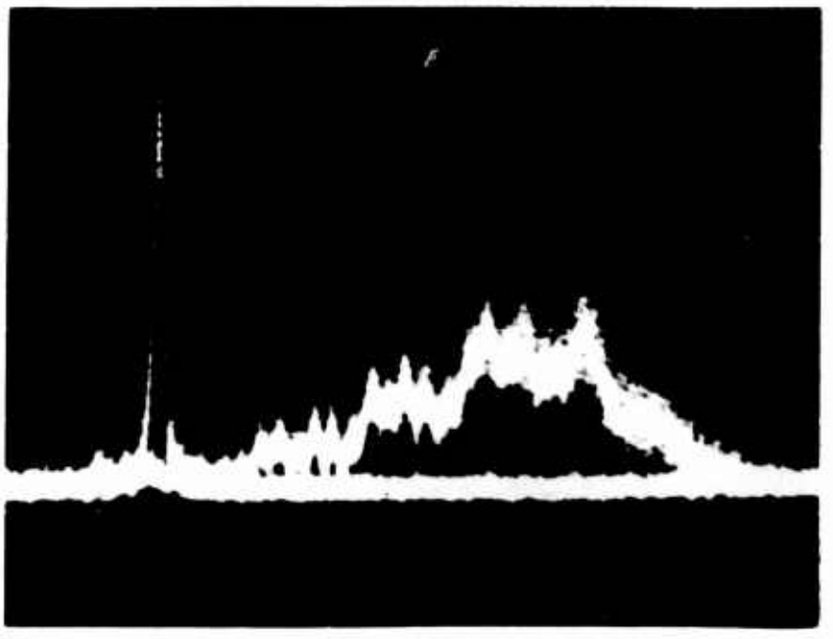

Figure 35. Double Exposure Showing Compressed and Uncompressed Pulses On Same Time and Amplitude Scale. (10 ns/div)

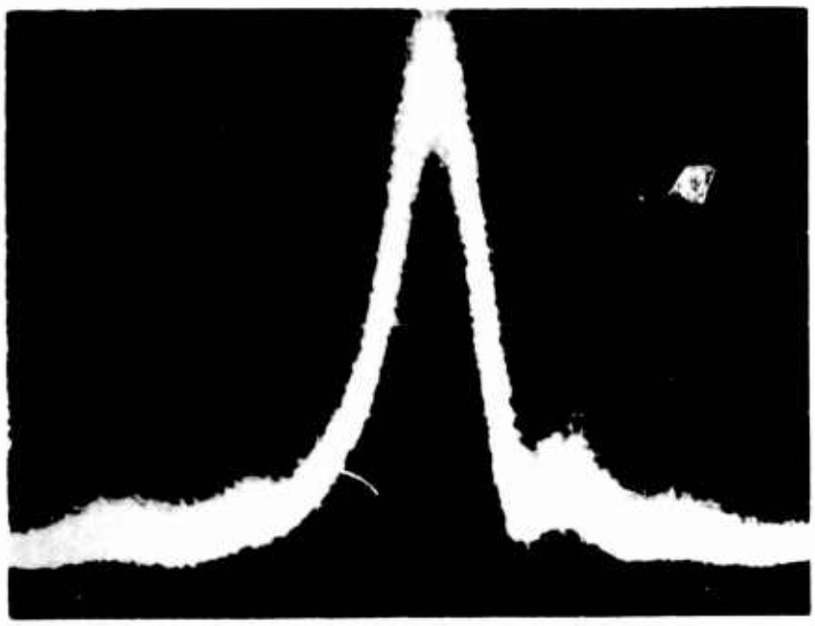

Figure 36 Compressed Pulse (1 ns/div)

D. CONCLUSIONS

The average insertion loss of the TML is approximately 6 db over the 1-2 Gc. frequency band. This figure is lower than either of the two filter types tested previously and results in a compressed pulse of about 7 db greater amplitude than the peak of the input pulse. The TML can be made into a more solid structure than the one shown by using a low-loss material such as Styrofoam to separate the two halves of the filter. An additional improvement would be to completely enclose the structure in a conductor to decrease RF leakage.

The two factors which limit the accuracy to which a desired delay-frequency characteristic may be achieved appear to be the coarseness of the TML (number of radiating elements per unit length) and the dimensional accuracy of the elements. On the filter just described, the change in "a" from one element to the next was 0.060 inch at the low frequency end and 0.010 inch at the high frequency end. In view of the fact that dimensions can be held to an accuracy of better than 0.001 inch in the photo-etching process, this would suggest that a time-bandwidth product in excess of

500 might be possible with the TML technique. The increased number of elements in such a filter would probably provide improved accuracy of delay if the delay of any given frequency is compared with the total differential delay.

A disadvantage of the TML is its apparent inability to compress a downsweeping signal. It seems possible that some improvement in the technique might be found which would allow compression of both types of signals, but at present this can only be suggested as a possibility for future study.

It seems reasonable to expect that some other type of radiating structure might give comparable or better results when used as a compression filter. Pulfer, Reference 14, discusses the dispersive properties of broad-band antennas and shows some measurements made on a pair of spiral antennas using the impulse measuring technique (figure 2). He also states that measurements have shown broadside and end-fire log-periodic antennas, broad-band dipoles, T-fed slots, and horns, to be dispersive. This indicates that further studies of broad-band antennas for use as compression filters might be fruitful.

V. CONCLUSIONS

The filter types described in this report are only three of five which were investigated under this project. The other two types, the Helix* and the Folded Tape Meander Lines**, were each the subject of a preliminary investigation such as the ones described here. The results in the case of the Helix and Folded Tape seemed promising enough to justify a more thorough analysis, and a separate report was issued on each of these devices.

It seems likely that some of the techniques studied here could be very useful in specific applications. For example, the PCML appears to be a promising technique for applications requiring a small time-bandwidth product. This might include a broad-band compression filter composed of a TDL with a PCML at each tap. Such a design might make effective use of several PCML's in achieving an overall phase accuracy beyond the capability of a single PCML. Additionally, the ability to shape the passband of each of the individual filters represents an additional degree of freedom which should result in a larger peak-to-sidelobe ratio.

The results obtained here do not represent the ultimate performance of any of the techniques described. They do, however, provide some insight into the potential of each of the filter types. To this extent, the objective of this investigation has been achieved.

---

* Reference 2

** Reference 3

APPENDIX

DERIVATION OF PCML DELAY EQUATION

The equation relating phase and frequency is taken from Reference 9, page 182:

$$\cot^2 \frac{kA}{2} = \tan \frac{\theta}{2} \left[\frac{\Delta U(\frac{W}{D}, \theta)\, \Delta U\,(1-\frac{W}{D},\ \theta+\pi)}{\Delta U\,(1-\frac{W}{D},\ \theta)\, \Delta U(\frac{W}{D},\ \theta+\pi)} \right] \tag{A1}$$

where

$$k = \frac{\omega}{c_d} \tag{A2}$$

$$\theta = \beta D \tag{A3}$$

$$\Delta U(1-\frac{W}{D}, \theta) = 2 \int_0^{\alpha} \frac{\cos(1-\frac{\theta}{\pi})t}{\sqrt{\sin^2\alpha - \sin^2 t}}\, dt \tag{A4}$$

$$\alpha = \frac{\pi}{2}(1-\frac{W}{D}) \tag{A5}$$

Defining

$$X \triangleq \left[\frac{\Delta U(\frac{W}{D}, \theta)\, \Delta U(1-\frac{W}{D},\ \theta+\pi)}{\Delta U(1-\frac{W}{D},\ \theta)\, \Delta U(\frac{W}{D},\ \theta+\pi)} \right] \tag{A6}$$

and substituting Eqs. (A2) and (A3) into Eq. (A1), the delay equation is obtained by differentiating:

$$\frac{A}{2c_d} \left(2\cot\frac{A}{2c_d}\right) \left(-\csc^2\frac{A}{2c_d}\right) d\omega = X\left(\sec^2\frac{\theta}{2}\right)\left(\frac{D}{2}\right) d\beta + \left(\tan\frac{\theta}{2}\right) \frac{dX}{d\beta}\, d\beta \tag{A7}$$

The group velocity is

$$v_g = \frac{d\omega}{d\beta} \tag{A8}$$

Substituting Eq. (A8) into Eq. (A7), the normalized delay equation is obtained:

$$\frac{c_d D}{Av_g} = -2 \frac{\cos \frac{\omega A}{2c_d}}{\sin^3 \frac{\omega A}{2c_d}} \left[X \sec^2 \frac{\omega\theta}{2} + \left(\tan \frac{\theta}{2} \right) \frac{dX}{d\beta} \right]^{-1} \tag{A9}$$

The expressions X and $\frac{dX}{d\beta}$ can be evaluated by numerical integration of Eq. (A4). For the case D = 2W however, X = 1 and $\frac{dX}{d\beta} = 0$. Making use of the trigonometric identity

$$\sec^2 \frac{\theta}{2} = 1 + \tan^2 \frac{\theta}{2} \tag{A10}$$

and substituting from Eq. (A1),

$$\frac{c_d D}{Av_g} = -2 \frac{\cos \frac{\omega A}{2c_d}}{\sin^3 \frac{\omega A}{2c_d}} \left[1 + \cot^4 \frac{\omega A}{2c_d} \right]^{-1} , \quad D = 2W \tag{A11}$$

This reduces to

$$\frac{c_d D}{Av_g} = 2 \left[\frac{\sin \left(\frac{\omega A}{c_d} \right)}{1 + \cos^2 \left(\frac{\omega A}{c_d} \right)} \right] \tag{A12}$$

REFERENCES

1. V. E. Dunn, "A Pulse Compression Filter Employing a Microwave Helix", Stanford Electronics Laboratories Tech. Report No. 557-1, Oct. 1960.
2. V. E. Dunn, "Realization of Microwave Pulse Compression Filters by Means of Folded-Tape Meander Lines", Stanford Electronics Laboratories Tech. Report No. 557-3, Oct. 1962.
3. W. R. Kincheloe, "The Measurement of Frequency with Scanning Spectrum Analyzers", Stanford Electronics Laboratories Tech. Report No. 557-2, Oct. 1962.
4. "Proceedings of Symposium on Pulse Compression Techniques and Applications Tech. Documentary Report No. RADC-TDR-62-580, Techniques Lab., RADC, Research and Technology Div., Air Force Systems Command, Griffiss Air Force Base, N.Y., April, 1963. (Secret-Title Unclassified)
5. A. W. Rihaczek, "Introduction to Pulse Compression, Part I", Report No. TDR-169 (3250-43) TN-1 Part I, Electronics Research Lab., Aerospace Corp., El Segundo, Calif, Apr. 1963.
6. J. R. Klauder, et. al., "Theory and Design of Chirp Radars", Bell System Tech. Journ., 39, Jul. 1960, pp. 745-808.
7. C. E. Cook. "Transmitter phase Modulation Errors and Pulse Compression Waveform Distortion", Microwave Journal Vol. 6, No. 63-69, May 1963.
8. P. N. Butcher, "A Theoretical Study of Propagation Along Tape Ladder Lines", Proc. Instn. Elec. Engnrs., 104, B, Mar. 1957, pp. 169-176.
9. P. N. Butcher, "The Coupling Impedance of Tape Structures", Proc. Instn. Elec. Engnrs., 104, B, Mar. 1957, pp. 177-187.

10. H. W. Batten, et. al., "The Response of a Panoramic Receiver to CW and Pulse Signals", Technical Report No. 3, (DA-36-039-SC-15358), Electronic Defense Group, University of Michigan, June 1952.

11. S. B. Cohn, et. al., "Research On Design Criteria For Microwave Filters - Final Report", (Contract DA-36-039-SC-64625), Stanford Research Institute, Menlo Park, Calif., June 1957.

12. S. B. Cohn, et. al., "Strip Transmission Lines and Components - Final Report", (Contract DA-36-0390SC-63232), Stanford Research Institute, Menlo Park, Calif., Feb. 1957.

13. Norman R. Wild, et. al., "Handbook of Tri-Plate Microwave Components", Sanders Associates, Inc., Nashua, New Hampshire.

14. J. K. Pulfer, "Dispersive Properties of Broad Band Antennas," Proc. IRE, 49, Mar 1961, p. 644 (Correspondence).

UNCLASSIFIED

Security Classification

DOCUMENT CONTROL DATA - R&D

(Security classification of title, body of abstract and indexing annotation must be entered when the overall report is classified)

1 ORIGINATING ACTIVITY (Corporate author)

Stanford University
Stanford Techniques Lab

2a REPORT SECURITY CLASSIFICATION

Unclassified

2b GROUP

n/a

3 REPORT TITLE

A Study of Several Microwave Compression Filter Techniques

4 DESCRIPTIVE NOTES (Type of report and inclusive dates)

Final Report

5 AUTHOR(S) (Last name, first name, initial)

H. S. Hewitt
W. R. Kincheloe, Jr.
M. H. Musser

6 REPORT DATE	7a TOTAL NO OF PAGES	7b NO OF REFS
November 1964	59	14

8a CONTRACT OR GRANT NO	9a ORIGINATOR'S REPORT NUMBER(S)
AF30(602)-2985	
b PROJECT NO: 4505	
c: Task 450501	9b OTHER REPORT NO(S) (Any other numbers that may be assigned this report): RADC TDR 64-398
d	

10 AVAILABILITY/LIMITATION NOTICES

Releaseable to OTS

Qualified requestors may obtain copies of this report from DDC

11 SUPPLEMENTARY NOTES	12 SPONSORING MILITARY ACTIVITY
	Rome Air Development Center Griffiss AFB N Y

13 ABSTRACT

Linear passive filters which decrease the duration of a frequency modulated pulse ("pulse compression" filters) are finding increasing application in radar and scanning receiver systems. This report describes the design, construction, and performance of several compression filters intended for use in a particular scanning receiver. These filters were designed to compress pulses in which the frequency varies linearly with time between 1 Gc and 2 Gc, nominally at a rate of 2×10^{16} cps (20 Mc per sec per ns). Included in the discussion are the following filter types: 1. Dispersive Helix, 2. Folded Tape Meander Line (FTML), 3. Printed Circuit Meander Line (PCML), 4. Tapped Delay Line (TDL), and 5. Radiation-Coupled Tapered Meander Line (TML). A description of the construction techniques and performance of the FTML, the PCML, and the TML is included in this report, while the helix and FTML are described in separate reports issued under this contract. The intent of this report is not to exhaustively treat each type of filter, but rather to provide a variety of possible approaches to compression filter realization, to provide design information, and to weigh some of the advantages of each type of filter and disadvantages. Although the filters described here are designed for a particular scan rate and frequency range, a similar approach could be used over a wide range of system parameters. With this in mind, an effort has been made to present design data in such a way as not to limit its generality or applicability.

DD FORM 1 JAN 64 1473

UNCLASSIFIED

Security Classification

14. KEY WORDS	LINK A		LINK B		LINK C	
	ROLE	WT	ROLE	WT	ROLE	WT
Pulse Compression Filters (Electromagnetic Wave) L-Band						

INSTRUCTIONS

1. ORIGINATING ACTIVITY: Enter the name and address of the contractor, subcontractor, grantee, Department of Defense activity or other organization *(corporate author)* issuing the report.

2a. REPORT SECURITY CLASSIFICATION: Enter the overall security classification of the report. Indicate whether "Restricted Data" is included. Marking is to be in accordance with appropriate security regulations.

2b. GROUP: Automatic downgrading is specified in DoD Directive 5200.10 and Armed Forces Industrial Manual. Enter the group number. Also, when applicable, show that optional markings have been used for Group 3 and Group 4 as authorized.

3. REPORT TITLE: Enter the complete report title in all capital letters. Titles in all cases should be unclassified. If a meaningful title cannot be selected without classification, show title classification in all capitals in parenthesis immediately following the title.

4. DESCRIPTIVE NOTES: If appropriate, enter the type of report, e.g., interim, progress, summary, annual, or final. Give the inclusive dates when a specific reporting period is covered.

5. AUTHOR(S): Enter the name(s) of author(s) as shown on or in the report. Enter last name, first name, middle initial. If military, show rank and branch of service. The name of the principal author is an absolute minimum requirement.

6. REPORT DATE: Enter the date of the report as day, month, year, or month, year. If more than one date appears on the report, use date of publication.

7a. TOTAL NUMBER OF PAGES: The total page count should follow normal pagination procedures, i.e., enter the number of pages containing information.

7b. NUMBER OF REFERENCES: Enter the total number of references cited in the report.

8a. CONTRACT OR GRANT NUMBER: If appropriate, enter the applicable number of the contract or grant under which the report was written.

8b, 8c, & 8d. PROJECT NUMBER: Enter the appropriate military department identification, such as project number, subproject number, system numbers, task number, etc.

9a. ORIGINATOR'S REPORT NUMBER(S): Enter the official report number by which the document will be identified and controlled by the originating activity. This number must be unique to this report.

9b. OTHER REPORT NUMBER(S): If the report has been assigned any other report numbers *(either by the originator or by the sponsor)*, also enter this number(s).

10. AVAILABILITY/LIMITATION NOTICES: Enter any limitations on further dissemination of the report, other than those imposed by security classification, using standard statements such as:

(1) "Qualified requesters may obtain copies of this report from DDC."

(2) "Foreign announcement and dissemination of this report by DDC is not authorized."

(3) "U. S. Government agencies may obtain copies of this report directly from DDC. Other qualified DDC users shall request through

_____."

(4) "U. S. military agencies may obtain copies of this report directly from DDC. Other qualified users shall request through

_____."

(5) "All distribution of this report is controlled. Qualified DDC users shall request through

_____."

If the report has been furnished to the Office of Technical Services, Department of Commerce, for sale to the public, indicate this fact and enter the price, if known.

11. SUPPLEMENTARY NOTES: Use for additional explanatory notes.

12. SPONSORING MILITARY ACTIVITY: Enter the name of the departmental project office or laboratory sponsoring *(paying for)* the research and development. Include address.

13. ABSTRACT: Enter an abstract giving a brief and factual summary of the document indicative of the report, even though it may also appear elsewhere in the body of the technical report. If additional space is required, a continuation sheet shall be attached.

It is highly desirable that the abstract of classified reports be unclassified. Each paragraph of the abstract shall end with an indication of the military security classification of the information in the paragraph, represented as *(TS), (S), (C), or (U)*.

There is no limitation on the length of the abstract. However, the suggested length is from 150 to 225 words.

14. KEY WORDS: Key words are technically meaningful terms or short phrases that characterize a report and may be used as index entries for cataloging the report. Key words must be selected so that no security classification is required. Identifiers, such as equipment model designation, trade name, military project code name, geographic location, may be used as key words but will be followed by an indication of technical context. The assignment of links, rules, and weights is optional.